

1 **Location and function of *Plasmodium* kinesins: key roles in parasite proliferation,**  
2 **polarity, and transmission**

3  
4 Mohammad Zeeshan<sup>1\*</sup>, Ravish Rashpa<sup>2†</sup>, David J Ferguson<sup>3,4†</sup>, Steven Abel<sup>5†</sup>, Zeinab  
5 Chahine<sup>5</sup>, Declan Brady<sup>1</sup>, Sue Vaughan<sup>3</sup>, Carolyn A. Moores<sup>6</sup>, Karine G. Le Roch<sup>5</sup>,  
6 Mathieu Brochet<sup>2</sup>, Anthony A. Holder<sup>7</sup> and Rita Tewari<sup>1\*</sup>

7  
8  
9 <sup>1</sup>University of Nottingham, School of Life Sciences, Nottingham, United Kingdom.

10 <sup>2</sup>University of Geneva, Faculty of Medicine, Geneva, Switzerland.

11 <sup>3</sup>Oxford Brookes University, Department of Biological and Medical Sciences, Oxford,  
12 United Kingdom.

13 <sup>4</sup>University of Oxford, John Radcliffe Hospital, Nuffield Department of Clinical Laboratory  
14 Science, Oxford, United Kingdom.

15 <sup>5</sup>Department of Molecular, Cell and Systems Biology, University of California Riverside,  
16 900 University Ave., Riverside, USA.

17 <sup>6</sup>Institute of Structural and Molecular Biology, Department of Biological Sciences,  
18 Birkbeck College, London, United Kingdom.

19 <sup>7</sup>The Francis Crick Institute, Malaria Parasitology Laboratory, London, United Kingdom.

20  
21  
22 †Contributed equally

23 \*For correspondence

24 Rita Tewari: [rita.tewari@nottingham.ac.uk](mailto:rita.tewari@nottingham.ac.uk)

25 Mohammad Zeeshan: [zeeshanmf@gmail.com](mailto:zeeshanmf@gmail.com)

26  
27  
28  
29  
30  
31  
32 **Short title:** Genome-wide analysis of *Plasmodium* kinesins

48 **Abstract**

49

50 Kinesins are microtubule-based motors important in cell division, motility, polarity and  
51 intracellular transport in many eukaryotes, but poorly studied in eukaryotic pathogens.  
52 *Plasmodium spp.*, the causative agents of malaria, are divergent eukaryotes with atypical  
53 aspects of cell division and plasticity of morphology throughout the lifecycle in both  
54 mammalian and mosquito hosts. Here we describe a genome-wide screen of  
55 *Plasmodium* kinesins, revealing diverse subcellular locations and functions in spindle  
56 assembly, axoneme formation and cell morphology. Surprisingly, only kinesin-13 has an  
57 essential role for growth in the mammalian host while the other eight kinesins are  
58 required during the proliferative and invasive stages of parasite transmission through the  
59 mosquito vector. In-depth analyses of kinesin-13 and kinesin-20 revealed functions in  
60 microtubule dynamics during apical polarity formation, spindle assembly and axoneme  
61 biogenesis. This comprehensive study will inform the targeting of microtubule motors for  
62 therapeutic intervention in malaria.

63

64

65

## 66 Introduction

67

68 Kinesins are microtubule (MT)-based motor proteins that use energy from the hydrolysis  
69 of ATP and function in various cellular processes including intracellular transport, mitotic  
70 spindle formation and chromosome segregation during cell division, and the organisation  
71 of cell polarity and cytoskeletal features associated with motility (Konjikusic et al., 2021;  
72 Verhey and Hammond, 2009). There are 14 to 16 kinesin subfamilies categorised in  
73 eukaryotes according to the primary sequences of the motor domain, with similar  
74 biological roles also established by *in vitro* studies, and *in vivo* phenotypes for subfamily  
75 members (Hirokawa and Tanaka, 2015; Konjikusic et al., 2021; Yount et al., 2015).  
76 Kinesin subfamilies that regulate MT dynamics, such as kinesin-8 and -13, are found in  
77 most eukaryotes including primitive and evolutionarily divergent eukaryotes (Vicente and  
78 Wordeman, 2015; Wickstead et al., 2010). Although there is an extensive literature with  
79 various bioinformatic and molecular investigations of kinesins, information on these  
80 molecular motors is sparse in deep rooted pathogenic eukaryotes including *Plasmodium*  
81 *spp.* and other Apicomplexa, *Giardia spp.*, and trypanosomes (Vicente and Wordeman,  
82 2015). These primitive eukaryotes have a flagellate stage in their life cycle and may have  
83 a complex MT-associated cytoskeleton (Wickstead and Gull, 2011) indicating the  
84 importance of MT-based motor proteins in their development.

85 *Plasmodium spp.*, the causative agents of malaria belong to the phylum  
86 Apicomplexa. They are ancient haploid unicellular eukaryotes with a number of  
87 morphologically diverse proliferative stages during the complex life cycle in various cells,  
88 tissues and organs of their vertebrate and invertebrate hosts (**Fig. 1A**) (Sinden, 1991;  
89 Zeeshan et al., 2020b). In the mammalian host the parasite proliferates within liver and  
90 red blood cells by repeated cycles of closed endomitotic division while retaining an intact  
91 nuclear membrane, with cytokinesis following the final nuclear division, in a process  
92 termed schizogony, to produce multiple infective haploid merozoites (**Fig. 1A**). In the  
93 cyclic, asexual proliferative blood stage, merozoites invade red blood cells (RBCs),  
94 developing through ring and trophozoite stages into schizonts (Sinden, 1991; Zeeshan et  
95 al., 2020b). DNA replication and asynchronous nuclear division form a polyploid cell  
96 followed by a final synchronised round of S-phase, karyokinesis and subsequent  
97 cytokinesis (Gubbels et al., 2020). Some of these haploid parasites in the RBC arrest  
98 and commit to sexual development as gametocytes (**Fig. 1A**). Gametocytes develop no  
99 further unless ingested in a blood meal by a female mosquito (the invertebrate host).  
100 Environmental conditions in the mosquito gut (lower temperature, higher alkalinity and  
101 the presence of xanthurenic acid) activate gametogenesis (Billker et al., 1998; Sinden et  
102 al., 1978). Female gametocytes produce a single, round, extracellular haploid female  
103 gamete 15 min after activation, without many apparent physiological or morphological  
104 changes (Sinden et al., 1978). Male gametogenesis is also very rapid and complete  
105 within 12 to 15 min after activation, but much more profound, with two major parallel  
106 events (Sinden et al., 1978). In three rounds of closed mitosis, DNA replication and  
107 chromosome segregation produce an 8N genome, which is followed by nuclear division  
108 and cytokinesis. In the cytoplasm axoneme assembly and maturation occur, leading to  
109 the formation of flagellate haploid male gametes in a process termed exflagellation  
110 (Sinden, 1991; Zeeshan et al., 2020b). The motile male gamete finds and fertilises the  
111 female gamete, and the resultant zygote differentiates through six distinct stages (I to VI)  
112 into a banana-shaped, invasive motile ookinete with a distinct apical polarity and conoid-  
113 associated proteins (Janse et al., 1985; Koreny et al., 2021; Zeeshan et al., 2020b). At  
114 the same time, in the first stage of meiosis, the DNA is duplicated and the now tetraploid  
115 ookinete develops over a 24 h period in the mosquito gut (Janse et al., 1985; Zeeshan et

116 al., 2020b), before traversing the mosquito gut wall and forming an oocyst under the  
117 basal lamina. Within the oocyst, sporogony, which is a form of endomitosis, produces  
118 many haploid sporozoites (Schrevel et al., 1977; Sinden and Strong, 1978). Sporozoites  
119 are motile and invasive polarised cells that migrate to and invade the salivary glands, so  
120 that the bite of the infected mosquito injects them into the next mammalian host  
121 (Graumans et al., 2020). Overall, the complete life cycle of the malaria parasite is  
122 characterised by varied morphological differences in size and shape, together with  
123 various modes of cell division and proliferation (**Fig. 1A**).

124 In a recent bioinformatic analysis of kinesins in Apicomplexa, we found nine  
125 kinesins encoded in the *Plasmodium berghei* genome, with members of three conserved  
126 kinesin subfamilies (kinesin-5, -8B, -8X and -13); kinesin-4, -15 and -20; and two  
127 Apicomplexa-enriched kinesins: kinesin-X3 and -X4 (Zeeshan et al., 2019b).  
128 Surprisingly, kinesin-5, -8X and -8B were not essential for blood stage proliferation  
129 (Zeeshan et al., 2020a; Zeeshan et al., 2019a; Zeeshan et al., 2019b). However, deletion  
130 of *kinesin-5*, which codes for a protein clearly co-located with the spindle apparatus in all  
131 proliferative stages, affected the production of infective sporozoites (Zeeshan et al.,  
132 2020a). Kinesin-8X was required for endomitotic proliferation in oocysts, and *kinesin-8B*  
133 deletion resulted in a defect in axoneme biogenesis during male gametogenesis (Depoix  
134 et al., 2020; Zeeshan et al., 2019a; Zeeshan et al., 2019b).

135 Here, we present a genome-wide screen of all *P. berghei* kinesins, including  
136 additional analyses of previously studied kinesin-5, -8B and -8X (Zeeshan et al., 2020a;  
137 Zeeshan et al., 2019a; Zeeshan et al., 2019b), using gene-targeting approaches, live-cell  
138 imaging, ultrastructure expansion microscopy and electron microscopy, and RNA-seq  
139 and ChIP-seq analyses. We examine the subcellular location of each kinesin using a  
140 protein endogenously tagged at the C-terminus with GFP, revealing a differential  
141 localisation of kinesins in mitotic and meiotic stages and a pellicular and polar location in  
142 certain invasive stages. Eight of the nine kinesin genes are required only for parasite  
143 transmission through the mosquito vector, during the sexual and sporogony stages. Only  
144 kinesin-13 is likely essential during blood stage schizogony. Kinesin-X3 and -X4, which  
145 are largely Apicomplexa-specific, show an interesting location on ookinete and  
146 sporozoite surface pellicle (-X3) and axonemes during male gametogenesis (-X4),  
147 respectively. These kinesins seem to have evolved in Apicomplexa for different MT-  
148 based structures such as the axoneme of flagella and a cytoskeletal scaffold to establish  
149 and maintain cell polarity, shape, and motility. An in-depth analysis of kinesin-13 and -20  
150 revealed distinct subcellular locations and functions in MT spindle assembly and  
151 formation, axoneme assembly and cell polarity. Kinesin-20 was associated with a striking  
152 ring-like structure during zygote to ookinete differentiation and deletion of the kinesin-20  
153 gene revealed a function in the morphology and motility of the ookinete. Ultrastructure  
154 expansion methods and electron microscopic analysis showed a defect arising from the  
155 extent and organization of subpellicular MTs. Kinesin-13 is expressed at all proliferative  
156 stages of the life cycle, and it associates with the kinetochore. A kinesin-13 genetic  
157 knockdown affected MT dynamics during spindle formation and axoneme assembly in  
158 male gametocytes, and subpellicular MT organization in ookinetes.

159 This comprehensive study of all *P. berghei* kinesins showed that most are  
160 required during parasite development within the mosquito vector where there are several  
161 morphological forms of the parasite cell, with differentiation between invasive and  
162 proliferative stages. Kinesin-13 is the only kinesin essential for both asexual blood  
163 stages and sexual stages. These findings will inform a strategy to target MT motors for  
164 therapeutic intervention against malaria.

## 166 Results

### 167 **Live-cell imaging of all *Plasmodium* kinesins reveals diverse locations during cell** 168 **division, differentiation, and pellicle formation throughout the life cycle.**

169 To investigate the expression and subcellular location of kinesins throughout the *P.*  
170 *berghei* life cycle, we generated transgenic parasite lines by single crossover  
171 recombination at the 3' end of each gene to express a fusion protein with a C-terminal  
172 GFP-tag (**fig. S1A**). PCR analysis of genomic DNA from each line, using locus-specific  
173 diagnostic primers, indicated correct integration of the GFP sequence (**fig. S1B**). Each  
174 kinesin-GFP parasite line completed the full life cycle with no detectable phenotypic  
175 change resulting from the GFP tagging. We analysed the expression and subcellular  
176 location of these GFP-tagged proteins by live cell imaging at various stages of the life  
177 cycle. Taken together with the previously published results for kinesin-5, -8B and -8X  
178 (Zeeshan et al., 2020a; Zeeshan et al., 2019a; Zeeshan et al., 2019b), we found that the  
179 nine kinesins have a diverse pattern of expression, with distinct subcellular locations  
180 including the mitotic spindle, axonemes, the surface pellicle and a polar distribution at  
181 various stages of the parasite life cycle (**Fig. 1B**). The diffuse distribution of kinesin-  
182 4GFP expression was detected only during oocyst development (**Fig. 1C**). Interestingly,  
183 only two kinesins, kinesin-5 and -13, were expressed throughout the parasite life cycle,  
184 including blood stage schizogony, and were located on the mitotic spindle in both  
185 asexual and sexual stages (**Fig. 1C**). Kinesin-5GFP was restricted to the nucleus and  
186 not detected in mature extracellular parasites such as merozoites, male gametes and  
187 sporozoites, while kinesin-13GFP had both a nuclear and cytoplasmic location (**Fig. 1C**).  
188 Kinesin-8XGFP was also located on the nuclear spindle but only during the proliferative  
189 stages within the mosquito vector. Three kinesins (kinesin-8B, -15 and -4X) were  
190 expressed only during male gametogenesis with cytosolic locations (**Fig. 1C**), and two  
191 kinesins (kinesin-20 and -X3) were first detected in female gametocytes with a diffuse  
192 location (**Fig. 1C**). Their presence continues into the zygote and later stages of ookinete  
193 differentiation and sporogony with particular locations that are discussed in detail below  
194 (**Fig. 1C**). We also observed two kinesins at polar locations: kinesin-8X at the basal end  
195 of stage V to VI ookinetes and kinesin-13 at the apical end throughout ookinete  
196 development (**Fig. 1C**). Overall, the phylogenetically conserved kinesin-5 and -8X are  
197 restricted to nuclear spindle and kinesin-13 is present in both nucleus and cytoplasm.  
198 The Apicomplexa-enriched kinesin-X3 and -X4 are confined to ookinete and sporozoite  
199 pellicle and flagellar axoneme, respectively.

### 201 **Kinesin-5 and -8X are nuclear spindle kinesins associated with the kinetochore** 202 **(NDC80) that bind centromeres.**

203 In our previous studies we showed that the location of two kinesins, -5 and -8X, is  
204 associated with spindles and restricted to the nucleus during most of the life cycle stages  
205 (Zeeshan et al., 2020a; Zeeshan et al., 2019b). To further examine the spatio-temporal  
206 dynamics of these kinesins during spindle formation, chromosome segregation and  
207 axoneme biogenesis during male gametogenesis, we crossed parasite lines expressing  
208 kinesin-5-GFP and -8X-GFP with lines expressing NDC80-Cherry, a kinetochore protein  
209 in the nucleus, and kinesin-8B-Cherry, an axonemal protein in the cytoplasm, and  
210 compared protein location by live-cell imaging. Both kinesin-5 and -8X (green) were co-  
211 localised with NDC80 (red) suggesting a role in mitotic spindle function and chromosome  
212 segregation (**Fig. 2A and B**). On the other hand, neither kinesin-5 nor kinesin-8X  
213 showed any overlap with cytosolic kinesin-8B (red) during male gametogenesis (**Fig.**  
214 **S2A and B**) confirming their restricted location within the nuclear compartment.

216 Kinetochores are multiprotein complexes assembled at the centromere of each  
217 chromosome, which mediate chromosome attachment to spindle MTs. Because kinesin-  
218 5 and -8X showed colocalization with kinetochore protein NDC80, we analysed further  
219 the binding of these proteins at the centromere DNA. We performed ChIP-seq  
220 experiments with parasites undergoing gametogenesis (6 min post-activation [mpa]),  
221 using kinesin-5GFP and -8XGFP tagged parasites and GFP-specific antibodies. Strong  
222 ChIP-seq peaks for each chromosome were observed with these kinesins, indicating  
223 their binding sites. Binding was restricted to a region close to the previously annotated  
224 centromeres of all 14 chromosomes (Iwanaga et al., 2012) and identical to those  
225 identified for *Plasmodium* Condensin and NDC80 studies (Pandey et al., 2020; Zeeshan  
226 et al., 2020b) (**Fig. 2C**). Together, live cell imaging and ChIP-seq analysis support the  
227 notion that kinesin-5 and -8X associate with kinetochores assembled at centromeres.

### 228 229 **Apicomplexa-enriched kinesins have discrete locations during pellicle formation** 230 **(-X3) and axoneme assembly (-X4) during sexual development.**

231 Previous bioinformatic analysis identified two divergent *Plasmodium* kinesins (kinesin-X3  
232 and -X4) (Wickstead et al., 2010; Zeeshan et al., 2019b); one of them (kinesin-X3) is  
233 restricted to the phylum Apicomplexa (Zeeshan et al., 2019b). Kinesin-X4 is also  
234 restricted to Apicomplexa except that it is also in the starlet sea anemone *Nematostella*  
235 *vectensis* (Wickstead et al., 2010). Parasitic organisms of Apicomplexa are characterised  
236 by a specialised apical structural complex that coordinates the interaction with and  
237 penetration of host cells, and have a surface pellicle comprised of the plasma membrane  
238 and an underlying layer of fused flattened membrane vesicles of the inner membrane  
239 complex (IMC) with associated MTs (Gould et al., 2008; Kono et al., 2013). To examine  
240 whether the kinesins are associated with these apicomplexan features, localisation by  
241 live cell imaging was performed. Kinesin-X3 and -X4 had a stage-specific expression  
242 during sexual development with a distinct location (**Fig. 1C**). During zygote to ookinete  
243 differentiation, kinesin-X3 expression was restricted to one side of the cell in the early  
244 stages of development (stage I-III), suggesting an involvement in pellicle formation (**Fig.**  
245 **3A**). In later stages (stage IV-VI), the kinesin-X3 location became more distinct around  
246 the periphery of the ookinete. Monoclonal antibody 13.1 conjugated with cy3 (red), which  
247 recognises the P28 protein on the surface of zygote and ookinete stages, stained these  
248 stages and colocalised with kinesin-X3 (green) (**Fig. 3A**), although kinesin-X3 was not  
249 present at the apical and basal ends of the developing ookinete (**Fig. 3A**). This suggests  
250 that kinesin-X3 is restricted to pellicle formation during ookinete and sporozoite stages in  
251 the mosquito.

252 Using live-cell imaging during male gametogenesis, the expression and location of  
253 kinesin-X4 (green) was compared with that of axonemal protein kinesin-8B (red) located  
254 on basal bodies and axonemes (Zeeshan et al., 2019a). Kinesin-X4 showed a diffuse  
255 cytosolic distribution during early stages of male gametogenesis (1-3 mpa) but no strong  
256 signal on the basal body tetrads labelled with kinesin-8B (red) (**Fig. 3B**). However, at 4-6  
257 mpa the kinesin-X4 signal distribution changed to resemble linear structures, which was  
258 maintained in the later stages (8-10 mpa) and showed co-localization with kinesin-8B  
259 (**Fig. 3B**). These data suggest that kinesin-X4 is located on axonemes together with  
260 kinesin-8B during flagella formation in *Plasmodium spp.*

### 261 262 **Genome-wide functional screen reveals that eight out of nine kinesins are required** 263 **only for parasite transmission and not for blood stage proliferation.**

264 Previously we described the functional roles during mosquito stages of three kinesins, -5,  
265 -8B and -8X; proteins that were not essential during blood stage development (Zeeshan

266 et al., 2020a; Zeeshan et al., 2019a; Zeeshan et al., 2019b). To study the function of the  
267 remaining six kinesins throughout the life cycle, each gene was deleted from *P. berghei*  
268 using a double crossover homologous recombination strategy as described previously  
269 (Tewari et al., 2010) (**Fig. S3A**). Successful integration of the targeting constructs at  
270 each gene locus was confirmed by diagnostic PCR (**Fig. S3B**), except that *kinesin-13*  
271 could not be deleted. PCR analysis of knockout parasites confirmed the complete  
272 deletion of these *kinesin* genes (**Fig. S3B**), indicating that they are not essential during  
273 the asexual blood stage. *kinesin-13*, which could not be deleted despite several  
274 attempts, likely has an essential role during the asexual blood stage. A recent functional  
275 profiling of the *P. berghei* genome (Bushell et al., 2017) also supports an essential role  
276 for kinesin-13 during the blood stage. This study found that five kinesins (kinesin-4, -8B, -  
277 8X, -20 and -X4) are not essential for blood stage growth but provided no data for  
278 kinesin-5, -15 and -X3 (Bushell et al., 2017).

279 Phenotypic analyses of these *kinesin*-knockout parasites, in comparison with the  
280 parental parasite (WTGFP), were carried out at various stages of the life cycle: in  
281 asexual blood stages, during male gametogenesis and the formation of exflagellation  
282 centres, during ookinete formation, in the number and size of oocysts, for the formation  
283 of sporozoites in oocysts and their migration to salivary glands, and for parasite  
284 transmission to the vertebrate host (**Fig. 4A**). Taken together with previously published  
285 studies on kinesin-5, -8B and -8X, only two knockout parasite lines ( $\Delta$ *kinesin-8B* and  
286  $\Delta$ *kinesin-15*) showed a defect in the formation of male gametes (**Fig. 4B**).  $\Delta$ *kinesin-8B*  
287 parasites produced no male gametes, as shown previously (Depoix et al., 2020;  
288 Zeeshan et al., 2019a), while there was a significant decrease in male gamete formation  
289 in  $\Delta$ *kinesin-15* parasites (**Fig. 4B**). Next, we analysed the zygote to ookinete transition  
290 (round to banana-shaped cells) after 24 h following gametocyte activation. Three  
291 parasite lines ( $\Delta$ *kinesin-8B*,  $\Delta$ *kinesin-15* and  $\Delta$ *kinesin-20*) produced no or reduced  
292 numbers of ookinetes (**Fig. 4C**).  $\Delta$ *kinesin-8B* parasites produced no ookinetes, as  
293 expected because there were no male gametes to fertilise the female gametes (**Fig. 4C**)  
294 (Zeeshan et al., 2019a).  $\Delta$ *kinesin-15* parasites produced significantly fewer male  
295 gametes, which would be expected to result in fewer ookinetes compared to WTGFP  
296 parasites (**Fig. 4C**). In contrast,  $\Delta$ *kinesin-20* parasites exflagellated normally and  
297 therefore loss of this kinesin must have a direct effect on ookinete formation (**Fig. 4C**).

298 To assess the effect of kinesin gene deletions on oocyst development and  
299 infective sporozoite formation, 40-50 *Anopheles stephensi* mosquitoes were fed on  
300 mice infected with individual *kinesin*-knockout lines, and parasite development was  
301 examined. First, GFP-positive oocysts on the mosquito gut wall were counted at 7-, 14-  
302 and 21-days post-infection (dpi). Three out of eight kinesin-knockout lines showed  
303 defects in oocyst production;  $\Delta$ *kinesin-8B* parasites produced no oocysts as shown  
304 previously (Zeeshan et al., 2019a), while there was a significant reduction in  $\Delta$ *kinesin-15*  
305 and  $\Delta$ *kinesin-20* oocysts compared to WTGFP oocysts at 7 dpi and a further reduction  
306 by 14 and 21 dpi (**Fig. 4D**). The adverse effects on ookinete production rather than a  
307 direct effect on oocyst development could explain this observation. Although there was  
308 no significant difference in the number of oocysts of other kinesin gene knockouts  
309 compared to WTGFP at 7 dpi, a significant reduction was observed for the  $\Delta$ *kinesin-8X*  
310 line at 14 dpi, which became more evident by 21 dpi (**Fig. 4D**). Oocyst size was not  
311 affected in most of the lines that produced them, the only exception was  $\Delta$ *kinesin-8X*  
312 oocysts, which were approximately half the size of WTGFP oocysts at 14 dpi, and even  
313 smaller by 21 dpi (**Fig. 4E**). It would appear that kinesin-8X is the only kinesin that  
314 directly affects oocyst development. Four out of eight kinesin-knockout lines produced  
315 no or defective sporozoites;  $\Delta$ *kinesin-8B* and  $\Delta$ *kinesin-8X* produced no sporozoites, as

316 reported earlier (Zeeshan et al., 2019a; Zeeshan et al., 2019b), while *Δkinesin-15* and  
317 *Δkinesin-20* lines had significantly reduced sporozoite numbers compared to control  
318 parental parasites (**Fig. 4F**). These defects were mirrored in the salivary glands: for the  
319 *Δkinesin-8B* and *Δkinesin-8X* lines no sporozoites were detected, as reported earlier  
320 (Zeeshan et al., 2019a; Zeeshan et al., 2019b), while *Δkinesin-15* and *Δkinesin-20*  
321 lines had a significantly reduced number. The *Δkinesin-5* parasite produced  
322 significantly fewer infective salivary gland sporozoites (**Fig. 4G**) as reported previously  
323 (Zeeshan et al., 2020a). However, although several kinesin gene-knockout lines  
324 exhibited defects in sporozoite production and reduced salivary gland infection, these  
325 sporozoites were still infectious to the mammalian host as observed with successful  
326 infection of new hosts in mosquito bite back experiments (**Fig. 4H**). In summary, for most  
327 of the kinesin gene-knockout *P. berghei* lines, there were clear developmental defects at  
328 specific stages of the life cycle within the mosquito vector.

### 329 **Kinesin-20-GFP location reveals a ring-like structure during ookinete** 330 **differentiation, and deletion of the kinesin-20 gene affects ookinete morphology** 331 **and motility.** 332

333 In the initial phenotypic screen described above, the *Δkinesin-20* parasite did not  
334 produce normal ookinetes (**Fig. 4C**) but did produce a few oocysts (**Fig. 4D**), so we  
335 undertook a more in-depth analysis to investigate this further. First, we analysed the  
336 spatiotemporal profile of kinesin-20GFP expression during zygote to ookinete  
337 differentiation, using P28 as a cell surface marker. Live cell imaging showed a diffuse  
338 distribution of kinesin-20GFP in the female gametocyte and zygote (**Fig. 1C, 5A**).  
339 Subsequently, the intensity of kinesin-20GFP increased in the developing apical  
340 protuberance from the main cell body, and at later stages, especially at stage-II and III  
341 that are about 6-8 h after gametocyte activation (**Fig. 5A**). The protein appeared like a  
342 ring restricted to the junction of the main cell body and the protrusion that is  
343 characteristic of developing ookinetes during stage II to stage V, and then largely  
344 disappeared in mature ookinetes (stage VI) with a largely diffuse distribution similar to  
345 that of the zygote stage (**Fig. 5A**).

346 Next, we examined the *Δkinesin-20* parasites to ascertain whether the zygote was  
347 formed and at what stage parasite development was blocked. The *Δkinesin-20* parasite  
348 developed a short protuberance in stage-II similar to that of the WTGFP control (**Fig.**  
349 **5B**), but this protrusion developed into a bulbous structure rather than the characteristic  
350 banana-shaped ookinete (**Fig. 5B**) and remained like this 24 h later when the WTGFP  
351 ookinete had fully differentiated into the banana-shaped structure (**Fig. 5B and C**). Since  
352 the mature wildtype ookinete is a motile and invasive stage, we investigated the motility  
353 of the *Δkinesin-20* bulbous ookinete using a Matrigel substrate, as described previously  
354 (Volkman et al., 2012; Zeeshan et al., 2019b). There was a significant decrease in the  
355 motility of *Δkinesin-20* ookinetes compared with the WTGFP ookinetes that showed  
356 normal gliding motility (**Fig. 5D and E; movies S1 and S2**).

357 Although *Δkinesin-20* parasites made no morphologically normal and motile  
358 ookinetes, nevertheless they formed a few oocysts that produced sporozoites (**Fig. 4F**).  
359 This would point to the mutation specifically affecting motility but not invasion of the  
360 mosquito gut. It is possible that a few immotile ookinetes may contact the mosquito gut  
361 wall during gut turbulence and these are able to invade and initiate oocyst formation. The  
362 *Δkinesin-20* sporozoites were morphologically similar to WTGFP parasites, so we  
363 examined their motility on Matrigel as described previously (Volkman et al., 2012; Wall  
364 et al., 2019). The motility of *Δkinesin-20* sporozoites was similar to that of WTGFP



sporozoites (**Fig. 5F and G; movies S3 and S4**), suggesting that the defect in *Δkinesin-20* parasite shape and motility is limited to ookinete development.

### **qRTPCR and RNA-seq analysis of *Δkinesin-20* parasites showed the modulation of a limited number of genes.**

In order to examine whether the expression of other kinesin genes is mis-regulated in *Δkinesin-20* parasites, we performed qRTPCR analysis of them. None of the other kinesin genes showed any significant change in expression in *Δkinesin-20* parasites compared with WTGFP parasites (**Fig. 5H**).

To determine genome-wide changes in transcription we performed RNA-seq analysis of the *Δkinesin-20* gametocytes at 2h post activation. The *kinesin-20* deletion in the *Δkinesin-20* strain was confirmed, since no significant reads mapped to this gene locus (**Fig. 5I**). The volcano plot shows that only one gene was upregulated, and 16 genes were down regulated (**Fig. 5J, Table S1A**). Most of the differentially regulated genes belong to *pir* and *fam* gene clusters localized in the telomeric and sub-telomeric regions. Two of the most downregulated genes (PBANKA\_1465700 and PBANKA\_0200600) in *Δkinesin-20* gametocytes belong to the *fam* gene cluster and were described as female gametocyte specific genes in a recent study (Reid et al., 2018). This suggests a link of kinesin-20 with female gametocyte development and function.

### **Ultrastructure analysis of *Δkinesin-20* ookinetes reveals disorganised subpellicular microtubules.**

The defective size and shape of *Δkinesin-20* parasites during ookinete differentiation led us to perform high resolution and ultrastructure analysis of the bulbous ookinetes using ultrastructure expansion- and electron microscopy. With expansion microscopy using MT-specific antibody, we observed a marked reduction in microtubule length (**Fig. 6A**): the length of MTs in *Δkinesin-20* bulbous ookinetes was decreased by approximately 40% compared to those of WTGFP parasites, a difference which also reflected a shortening of the overall length of the ookinete (**fig. S4**). This difference was confirmed by electron microscopy observations (**Fig. 6B**).

In an ultrastructural comparison of WTGFP and *Δkinesin-20* ookinetes, the most obvious difference was the shape of the cell. In longitudinal section, the WTGFP ookinetes were elongated with a crescentic outline (**Fig. 6Ba**), but in contrast, longitudinal sections of the *Δkinesin-20* ookinetes were less elongated and had a more bulbous appearance (**Fig. 6Bb, c**). In WTGFP parasites, the distribution of subcellular organelles appeared ordered with most micronemes in the apical cytoplasm, a more centrally located crystalline body and a posterior nucleus (**Fig. 6Ba**). In contrast, early *Δkinesin-20* ookinetes had a large central nucleus with a few dense granules but lacked both micronemes and a crystalline body (**Fig. 6Bb**). Others that appeared more mature, possessed similar organelles (micronemes, crystalline body, nucleus) to those of the WTGFP, but differed from the control in having more randomly distributed micronemes (**Fig. 6Bc**).

Due to the differences in cell shape, the apical complex and pellicle were examined in detail. When the apical complex was examined in longitudinal (**Fig. 6Bd, e**) and cross (**Fig. 6Bf, g**) section, the complex nature of the structure was revealed. Interestingly, WTGFP and *Δkinesin-20* ookinetes displayed an identical sub-structure (**Fig. 6Bd–e and f–g**). In longitudinal sections of the central apex region, three conoidal rings could be identified underneath the plasma membrane. A unique sub-structure of the ookinete is the apical collar, which represents a cone-like structure embedded

115 between the microtubules and IMC of the pellicle (Koreny et al., 2021). The outer region  
116 of the collar is electron dense and appears to be fused to the IMC, which is interrupted at  
117 the apical end to form apical polar ring 1 (**Fig. 6Bd-g**). The inner aspect of the collar is  
118 more electron lucent and in close contact with the sub-pellicular MTs (**Fig. 6Bd-g**). The  
119 apical ends of the MTs are attached to a ring forming apical polar ring 2 (**Fig. 6Bd, e**).  
120 For a detailed review of the apical complex see Koreny et al (Koreny et al., 2021).  
121 Approximately 50 sub-pellicular MTs emanate from polar ring 2 and run longitudinally  
122 beneath the collar (**Fig. 6Bf, g**) and then beneath the IMC of the pellicle (**Fig. 6Bh, i**). In  
123 the region of the collar, MTs were evenly distributed in both WTGFP and  $\Delta$ kinesin-20  
124 parasites (**Fig. 6Bf, g**), however, in more posterior sections, while there continued to be  
125 an even distribution of MTs in close contact with the IMC in the WTGFP (**Fig. 6Bh**)  
126 ookinete, in the  $\Delta$ kinesin-20 parasite there were areas where there was uneven  
127 distribution, clumping and detachment of the MT from IMC (**Fig. 6Bi**).  
128

### 129 **Kinesin-13 associates with kinetochore marker NDC80 at all proliferative stages of** 130 **the life cycle and its knockdown affects male gamete formation.**

131 Since kinesin-13 was the only kinesin gene that was essential for blood stage  
132 schizogony and could not be disrupted in our genome-wide screen (**Fig. 4**), we  
133 performed a detailed analysis of kinesin-13. We observed both a diffuse cytoplasmic  
134 distribution and a distinct nuclear pattern of kinesin-13GFP during all proliferative stages  
135 as shown in **Fig. 1**. First, we performed live cell co-imaging of kinesin-13GFP and the  
136 NDC80-cherry kinetochore marker after crossing the two transgenic parasite lines, to  
137 observe kinesin-13-GFP dynamics during chromosome segregation in various  
138 developmental stages. There was colocalization of kinesin-13 and NDC80 at all  
139 proliferative stages (**Fig. 7**), for example during the schizogony and sporogony  
140 endomitotic stages (**Fig. 7A, B**). In the sexual cells, during the rapid mitosis of male  
141 gametogenesis there was partial colocalization of kinesin-13 and NDC80, but a  
142 substantial amount of kinesin-13 was also located in the cytosolic compartment (**Fig.**  
143 **7C**). In the meiotic stage during ookinete development there was clear colocalization of  
144 kinesin-13 and NDC80 (**Fig. 7D**). At the start of meiosis (2 h after zygote formation) there  
145 was one strong nuclear focus and at the end of ookinete formation there were three to  
146 four co-localised foci (**Fig. 7D**). Further analysis by fixed immunofluorescence  
147 microscopy of kinesin-13 (green) in the male gamete revealed a co-localization with  
148 tubulin (red) (**Fig. S5A**). To further examine the location of kinesin-13, we used  
149 ultrastructure expansion microscopy to examine gametocytes activated for 15 min, and  
150 then compared its location with that of tubulins. Kinesin-13 (green) was observed to co-  
151 localized with  $\alpha/\beta$  tubulin (magenta) suggesting a location on axonemes and spindles  
152 (**Fig. S5B**).

153 Since, kinesin-13 is essential for the asexual blood stage, and the gene could not  
154 be deleted, we applied two conditional genetic knockdown strategies to evaluate its role  
155 at other proliferative stages within mosquito vector. First, we used an auxin-inducible  
156 degraon (AID) system to try and study the effect of rapid kinesin-13 degradation in  
157 gametocytes. We tagged the endogenous kinesin-13 gene with an AID/HA epitope tag  
158 (**Fig. S6A**) to degrade the fusion protein in presence of auxin (Philip and Waters, 2015),  
159 and successfully generated kinesin-13-AID parasite lines as shown by integration PCR  
160 (**Fig. S6B**) but could not deplete kinesin-13 protein by auxin treatment (**Fig. S6C**). Next,  
161 we used a promotor trap double homologous recombination (PTD) approach, inserting  
162 the *clag* promotor at the 5' end of kinesin-13, and generated the conditional knockdown  
163 parasite: P*clag*kinesin-13 (kinesin-13PTD) (**Fig. S6D**). The *clag* (cytoadherence-linked  
164 asexual gene) is highly expressed in asexual blood stages, but largely silent during

465 stages of sexual differentiation, including gametocytes and ookinetes (Sebastian et al.,  
466 2012). The successful insertion was confirmed by diagnostic PCR (**Fig. S6E**) and qRT  
467 PCR showed a significant downregulation of kinesin-13 gene transcripts in *kinesin-*  
468 *13PTD* gametocytes, when compared to WTGFP gametocytes (**Fig. 8A**).

469 The phenotype of the *kinesin-13PTD* modification was examined during various  
470 stages of the parasite life cycle. Parasite proliferation in asexual blood stages was not  
471 affected, but during male gametogenesis, exflagellation was markedly reduced and very  
472 few male gametes were produced by *kinesin-13PTD* parasites compared to WTGFP  
473 parasites (**Fig. 8B**). Zygote development and ookinete differentiation were severely  
474 affected, and no clear banana-shaped ookinetes were observed (**Fig. 8C**). Subsequent  
475 stages in the mosquito were also affected significantly and no oocyst or sporozoite  
476 formation was observed (**Fig. 8D**), and as a consequence no transmission of *kinesin-*  
477 *13PTD* parasites occurred, as shown by mosquito bite back experiments (**Fig. 8E**).

### 479 **Global transcriptomic analysis of *kinesin-13PTD* parasites shows mis-regulation** 480 **of transcripts for gene clusters involved in axoneme assembly and chromosome** 481 **dynamics.**

482 To examine the transcript level of other kinesins in *kinesin-13PTD* gametocytes, we  
483 performed qPCR for all the nine kinesins and found that some, like kinesin-8B, -8X, -15  
484 and -20, were downregulated (**Fig. 8F**).

485 Since transcripts of other kinesins were affected, global transcription was  
486 investigated by RNA-seq analysis of *kinesin-13PTD* gametocytes at 0 and 15 mpa,  
487 representing times point before the start of male gametogenesis and just after male  
488 gamete formation (exflagellation), respectively. *Kinesin-13* downregulation in *kinesin-*  
489 *13PTD* gametocytes, relative to WTGFP gametocytes, was confirmed by RNA-seq  
490 analysis, showing the lack of reads for this locus (**Fig. 8G**). In addition to reduced  
491 kinesin-13 expression, 34 other genes were significantly downregulated and the  
492 expression of 152 genes was significantly upregulated in *kinesin-13PTD* gametocytes  
493 before activation (at 0 mpa) (**Fig. 8H; Table S1B**). Similarly, the expression of 22 genes  
494 was significantly downregulated and the expression of 329 genes was significantly  
495 upregulated in *kinesin-13PTD* gametocytes after 15 min activation (**Fig. 8I; Table S1C**).  
496 Bioinformatic analysis of these differentially regulated genes revealed two important  
497 clusters of genes that were affected, including those coding for proteins involved in  
498 axoneme assembly, glideosome assembly and chromosome dynamics (**Fig. 8J**).

### 500 **High resolution ultrastructure analysis of *kinesin-13PTD* parasites identified** 501 **defects in spindle assembly and axoneme MT of gametocytes, and the** 502 **subpellicular MT of ookinetes.**

503 Phenotypic analysis of *kinesin-13PTD* parasites revealed defects in male gamete and  
504 ookinete formation, and therefore we performed comparative high resolution image  
505 analysis of *kinesin-13PTD* and WTGFP gametocytes and ookinetes. Ultrastructure  
506 expansion microscopy revealed that both spindle and axoneme MTs were disorganised,  
507 and no clear flagella were visible at 4 to 5 or 15 min after male gametocyte activation,  
508 respectively (**Fig. 9A**). Disorganised MT were also observed in the defective *kinesin-*  
509 *13PTD* zygotes/ookinetes in comparison to the corresponding WTGFP parasites (**Fig.**  
510 **9A**).

511 These data were substantiated by electron microscopy analysis of male  
512 gametocytes activated for 6 or 15 min (**Fig. 9B**). The electron micrographs showed that  
513 in both WTGFP and *kinesin-13PTD* parasites at 6 mpa, most male gametocytes were at  
514 early stage of development, with a spherical appearance and a large central nucleus

515 **(Fig. 9Ba, c)**. In WTGFP gametocytes, a number of nuclear poles were observed while  
516 the cytoplasm contained a number of normal 9+2 axonemes, and some abnormal  
517 axonemes **(Fig. 9Ba, b)**. Although in the *kinesin-13PTD* gametocytes few nuclear poles  
518 were observed **(Fig. 9Bc)**, the major difference was in the cytoplasm, where there were  
519 collections of free single and double MTs plus a number partially organized into  
520 axonemes-like structures **(Fig. 9Bd)** while 9+2 axonemes were very rare. At 15 mpa, in  
521 the WTGFP samples, a number of late stages were observed with evidence of  
522 exflagellation and protruding microgametes **(Fig. 9Be)**. A number of free male gametes  
523 complete with nucleus and flagellum was observed **(Fig. 9Bf, g)**. In contrast, in the  
524 *kinesin-13PTD* parasites, the majority of male gametocytes were still at an early stage,  
525 and in the few at a later stage, the nucleus displayed clumps of chromatin **(Fig. 9Bh)**  
526 with a few examples of protrusions of MTs from the plasma membrane **(Fig. 9Bi)**, but  
527 with no evidence of flagella formation or free male gametes.

528  
529

## 530 Discussion

531 *Plasmodium spp.* have a complex life cycle involving two hosts. They invade tissues and  
532 cells in diverse environments and have evolved a series of cellular shapes and sizes,  
533 with several distinct morphological forms with cellular polarity and gliding motility for  
534 invasion, and cellular proliferation underpinned with an atypical mode of cell division  
535 (Gubbels et al., 2020; Sinden, 1991; Zeeshan et al., 2020b). Many of these processes  
536 are governed by MTs and MT-based motor proteins like kinesins (Zeeshan et al.,  
537 2019b). In many organisms including *Plasmodium spp.*, MTs form different structural  
538 frameworks such as the spindle assembly during cell division, the axonemes of cilia and  
539 flagella, and a cytoskeletal scaffold to establish and maintain cell polarity, cell shape,  
540 intracellular transport, and cell motility (Morrissette and Sibley, 2002; Spreng et al.,  
541 2019). Kinesins regulate the organisation and function of MTs, using them as a track for  
542 movement or regulating their dynamics during cellular processes (Verhey and  
543 Hammond, 2009; Vicente and Wordeman, 2015). *Plasmodium spp.* are evolutionarily  
544 divergent unicellular eukaryotes with genomes that encodes nine kinesins including two  
545 that are Apicomplexa-enriched, and which lack three classical kinesins (kinesin-1, -2 and  
546 -3) normally important in intracellular transport (Wickstead et al., 2010; Zeeshan et al.,  
547 2019b). In the present study we performed a systematic comparative analysis of the  
548 timing of expression and subcellular location of all kinesins, and their roles in parasite  
549 proliferation, polarity and transmission throughout the life cycle. This comprehensive  
550 study also included the three previously described kinesins (Kinesin-5, -8B and -8X).  
551 (Zeeshan et al., 2020a; Zeeshan et al., 2019a; Zeeshan et al., 2019b).

552 The expression and subcellular location of each kinesin provides important  
553 information about their potential role. Three of the most evolutionarily conserved kinesins  
554 (kinesin-5, -8X and -13) are abundant throughout the life cycle with a similar location on  
555 spindles and associated with the kinetochore protein NDC80, consistent with a role in  
556 spindle dynamics during endomitosis and meiosis, as shown in our recent studies  
557 (Zeeshan et al., 2020a; Zeeshan et al., 2019b). Kinesin-13 is the most widely expressed  
558 of these motors in all proliferative and invasive stages, with diverse cytoplasmic locations  
559 including axonemes in male gametocytes and at the apical end of the differentiating  
560 ookinete in addition to its association with the nuclear spindle apparatus. A similar  
561 diverse set of kinesin-13 locations has been reported in other eukaryotes (Ali et al.,  
562 2017; Ems-McClung and Walczak, 2010; Manning et al., 2007), highlighting its  
563 importance for various MT-associated biological processes in *Plasmodium spp.*

564 Male gametogenesis in *Plasmodium spp.* is a rapid process that includes three  
565 rounds of genome replication with successive spindle formation and cytoplasmic  
566 axoneme assembly before karyokinesis and cytokinesis, and all completed within 12-15  
567 min of gametocyte activation (Sinden et al., 1978). The cytoplasmic location of three  
568 male gametocyte-specific kinesins (kinesin-8B, -15 and -X4) and kinesin-13, highlights  
569 the importance of these kinesins for rapid axoneme assembly and flagellum formation in  
570 *Plasmodium spp.*, especially kinesin-X4. This motor is phylogenetically largely restricted  
571 to Apicomplexa and displays a male gametocyte-specific expression with an axonemal  
572 location. Kinesin-X4 colocalizes with kinesin-8B but is not essential like kinesin-8B,  
573 suggesting that it might be complementing the role of kinesin-8B (Zeeshan et al., 2019a).  
574 In addition to Apicomplexa, kinesin-X4 is found in the starlet sea anemone *Nematostella*  
575 *vectensis*, where its function is also unknown (Wickstead et al., 2010). The axonemes  
576 are assembled directly in the male gametocyte cytoplasm and, thus, there is no  
577 requirement for transport of building materials by the intraflagellar transport (IFT)  
578 mechanisms common in many other eukaryotes (Briggs et al., 2004; Mirvis et al., 2018;  
579 Sinden et al., 2010). *Plasmodium spp.* male gametes have a very simple structure,

580 consisting of an electron dense basal body that lacks the classical nine triplet MTs (9+0)  
581 connected to an axoneme with a typical 9+2 MT organization associated with dynein,  
582 with an adjacent elongated nucleus all enclosed within the plasma membrane (Okamoto  
583 et al., 2009; Sinden et al., 1978). In a previous *Plasmodium berghei* male gamete  
584 proteome study, three kinesins (kinesin-8B, -13 and -15) were identified and proposed to  
585 have an important role in axoneme assembly (Talman et al., 2014). In a recent study on  
586 the regulation of *P. berghei* male gametogenesis, a large number of phospho-regulated  
587 proteins have motor activity, and they include most of these kinesins (Invergo et al.,  
588 2017). The expression of six kinesins (kinesin-5, -8B, -8X, -13, -15, and -X4) in  
589 gametocytes and their location in either nucleus (kinesin-5 and -8X), cytoplasm (kinesin-  
590 8B, -15, and -X4) or both (kinesin-13) suggest the importance of these kinesins in male  
591 gametogenesis and thus parasite transmission.

592 The restricted location of kinesin-X3 at the pellicle of ookinetes, except for the  
593 apical and basal ends of the cell, suggests an involvement in subpellicular MT/IMC  
594 interactions. The absence of kinesin-X3 from the apical end highlights that it is not a part  
595 of the conoidal complex (Bertiaux et al., 2021; Koreny et al., 2021). Kinesin-20 has a  
596 ring-like location at the junction between the protrusion and the main cell body of the  
597 developing ookinete, suggesting a role in formation of the IMC/sub-pellicular microtubule  
598 complex and defining the size and shape of the cell, and then disappears from the  
599 mature cell. *Plasmodium* Myosin F has a similar location in early stages of ookinete  
600 development (Wall et al., 2019) suggesting the existence of an actomyosin contractile  
601 ring that might be regulated by kinesin-20.

602 Genetic analysis revealed that most of the kinesins (8 out of 9) have their most  
603 important roles in transmission stages within the mosquito, where there are substantial  
604 changes in cell size, morphology, and invasive properties, which may be regulated by  
605 MTs and associated proteins. For example, the results of our ultrastructural analysis of  
606  $\Delta$ kinesin-20 parasites show that loss of this kinesin affects the development of ookinete  
607 shape and size. MTs length, number and association with the IMC are crucial to  
608 determine the size, shape and motility of certain *Plasmodium spp.* stages (Spreng et al.,  
609 2019). We show that kinesin-20 regulates the length and arrangement of subpellicular  
610 MTs of developing ookinetes. Subpellicular MTs along with IMC proteins maintain  
611 ookinete polarity and morphology in *Plasmodium spp.* (Kono et al., 2013). IMC1b-  
612 deficient ookinetes display abnormal cell shape and reduced gliding motility (Trempe  
613 et al., 2008) similar to the properties of  $\Delta$ kinesin-20, and a similar phenotype was observed  
614 in a recent study showing that palmitoylation of IMC subcompartment proteins (ISPs)  
615 regulates the apical subpellicular MT network in ookinetes and affects their elongation  
616 (Wang et al., 2020). ISPs also maintain the polar location of guanylate cyclase beta  
617 (GC $\beta$ )/CDC50A complex at the IMC, essential for ookinete gliding (Gao et al., 2018).  
618 PPKL-deficient parasites have a defective MT organisation and abnormal shaped  
619 ookinetes (Guttery et al., 2012), but the  $\Delta$ kinesin-20 phenotype is slightly different, with  
620 no defect in the apical ring, which serves as an MT organising centre for subpellicular  
621 MTs, and similar to what was found for phosphodiesterase- $\delta$  (*pde $\delta$* ) deficient ookinetes,  
622 which lack this enzyme involved in cyclic GMP signaling (Moon et al., 2009). The  
623 kinesin-20GFP location suggests there is a ring-like structure at the junction of the  
624 protrusion and cell body, which defines the developing ookinete shape and diameter,  
625 while apical polarity guides ookinete size and differentiation. An actomyosin contractile  
626 ring is present in elongation of embryonic cells of *Ciona intestinalis*, a primitive chordate  
627 (Sehring et al., 2014). The assembly and organization of an actomyosin contractile ring  
628 during cytokinesis is highly dynamic and contains, in addition to actin and myosin, other  
629 proteins that regulate actin nucleation, cross-linking and myosin activity (Mangione and

530 Gould, 2019; Vavylonis et al., 2008). In *Plasmodium spp.* and other members of  
531 Apicomplexa, a similar contractile ring has been reported as required for cytokinesis  
532 (Hammarton, 2019; Morano and Dvorin, 2021) but an involvement in cell elongation is  
533 unknown. Kinesin-20 could be a protein that regulates contractile ring function in cell  
534 elongation during ookinete development.

535 The in-depth structural analysis of *kinesin-13PTD* parasites reveals the  
536 importance of kinesin-13 in regulating MT organisation in sexual stages in the mosquito.  
537 Kinesin-13s are MT depolymerising kinesins, playing essential roles in spindle MT  
538 dynamics, kinetochore-MT attachment, and chromosome segregation (Ali et al., 2017;  
539 Ems-McClung and Walczak, 2010; Manning et al., 2007). *Plasmodium falciparum*  
540 kinesin-13 has also been shown to exhibit MT depolymerisation activity *in vitro* (Moores  
541 et al., 2002). Kinesin-13 homologs are present in most eukaryotes possessing cilia or  
542 flagella (Wickstead and Gull, 2006) and regulate the length of these structures (Chan  
543 and Ersfeld, 2010; Piao et al., 2009; Vasudevan et al., 2015). The knockdown of  
544 *Plasmodium berghei* kinesin-13 resulted in defects in the organisation of both spindle  
545 and axonemal MTs, thus arresting nuclear division and axoneme assembly during male  
546 gametogenesis. A similar phenotype was observed for the kinesin-8B gene knockout,  
547 which shows defective basal body formation and axoneme assembly during male  
548 gametogenesis, but nuclear division was normal (Zeeshan et al., 2019a). Knockout of  
549 the gene for another basal body protein, SAS6, resulted in a similar phenotype with  
550 defective basal body formation and axoneme assembly but no effect on nuclear division  
551 (Marques et al., 2015). Disruption of the gene for PF16, an armadillo-repeat protein of  
552 *Plasmodium spp.*, produces a similar phenotype, with an effect on axonemal central MT  
553 assembly and male gamete motility and fertility (Straschil et al., 2010). We found a  
554 *cdc2*-related kinase (CRK5) that is important for nuclear spindle formation but has no  
555 effect on axoneme assembly during male gametogenesis (Balestra et al., 2020).  
556 Previous studies have shown a similar phenotype for CDPK4, SRPK and MAP2 gene  
557 disruptions, where either the early or late stages of exflagellation are impaired but  
558 axoneme assembly is not (Fang et al., 2017; Tewari et al., 2005; Tewari et al., 2010). In  
559 another primitive eukaryote, *Giardia intestinalis*, kinesin-13 regulates MT dynamics  
560 during both flagellar assembly and nuclear division (Dawson et al., 2007).

561 Since kinesin-13 was not completely depleted, a few male gametes were  
562 produced that fertilised female gametes to form zygotes. However, these zygotes did not  
563 transform to ookinetes and produced only abnormal forms or ones arrested at the  
564 undifferentiated (retort) stage. Ultrastructure analysis of these retorts revealed a loss of  
565 polarity and disorganisation of the subpellicular MTs, consistent with the additional polar  
566 localization of kinesin-13GFP in zygotes and during ookinete development. This  
567 phenotype of kinesin-13 depletion is different from that of the kinesin-20 knockout  
568 (described above), where the apical polarity was not affected. A similar phenotype has  
569 been observed following the knockdown of two *P. berghei* phosphatases, PPKL and  
570 PP1, where apical polarity was lost, affecting ookinete differentiation (Guttery et al.,  
571 2012; Zeeshan et al., 2021).

572 Global transcriptomic analysis supported these findings with kinesin-13, as the  
573 expression of several genes involved in chromosome segregation, axoneme biogenesis,  
574 IMC/glideosome formation and other biological processes were modulated in *kinesin-13PTD*  
575 parasites. For example, differentially expressed genes like CRK5, SRPK, CDPK4  
576 are involved in chromosome segregation during male gametogenesis (Fang et al., 2017;  
577 Tewari et al., 2005; Tewari et al., 2010). Kinesin-8B, kinesin-X4, dynein and radial spoke  
578 proteins are involved in axoneme assembly, male gamete formation and fertility  
579 (Andreadaki et al., 2020; Talman et al., 2014; Zeeshan et al., 2019a). Differential

580 expression of genes like IMCs and GAPs indicates the additional role of kinesin-13 in  
581 glideosome formation and motility. Most of these changes in gene expression are  
582 obvious at 15 min post activation of gametocytes prior to gamete formation and  
583 fertilization. Translation repression in *Plasmodium spp.* is released after fertilization,  
584 allowing the stored transcripts in female gametocytes to be translated to form proteins  
585 essential for zygote development and ookinete invasion (Mair et al., 2006). Differential  
586 expression, mainly upregulation of these genes in *kinesin-13PTD* parasites, suggests a  
587 compensatory role during male gametogenesis and ookinete formation. Overall, these  
588 global transcriptomic data for *kinesin-13PTD* parasites are consistent with the profound  
589 phenotypic changes observed during male gametogenesis and ookinete formation.

590 In conclusion, the nine *P. berghei* kinesins show a diverse pattern of expression  
591 and subcellular location at various stages of the parasite life cycle. Genetic and  
592 phenotypic analyses indicate that most kinesins have their most important roles in  
593 mosquito stages, except kinesin-13 which is also essential for asexual blood stages (**Fig.**  
594 **10**). Kinesin-20 and kinesin-13 have roles in MT dynamics during proliferation, polarity  
595 formation, and transmission of the parasite. It will be interesting in the future to look for  
596 the interacting partners of these kinesins, to understand their mechanisms of action  
597 during these biological processes. This comprehensive study provides knowledge and  
598 understanding of the important roles of kinesins in various cellular processes at different  
599 stages of the life cycle of this evolutionarily divergent eukaryotic pathogen. This  
700 information may be useful to exploit kinesins as promising targets for therapeutic  
701 intervention against malaria.



## 704 **Materials and Methods**

### 706 **Ethics statement**

707 The animal work passed an ethical review process and was approved by the United  
708 Kingdom Home Office. Work was carried out under UK Home Office Project Licenses  
709 (30/3248 and PDD2D5182) in accordance with the UK 'Animals (Scientific Procedures)  
710 Act 1986'. Six- to eight-week-old female CD1 outbred mice from Charles River  
711 laboratories were used for all experiments.

### 713 **Generation of transgenic parasites and genotype analyses**

714 To observe the location of kinesin proteins, the C-terminus was tagged with green  
715 fluorescent protein (GFP) sequence by single crossover homologous recombination at  
716 the 3' end of the gene. To generate the GFP-tag line, a region of these genes  
717 downstream of the ATG start codon was amplified, ligated to p277 vector, and  
718 transfected as described previously (Guttery et al., 2012). The p277 vector contains the  
719 human *dhfr* cassette, conveying resistance to pyrimethamine. A schematic  
720 representation of the endogenous gene locus, the constructs and the recombined gene  
721 locus can be found in **Fig S1A**. For the parasites expressing a C-terminal GFP-tagged  
722 protein, diagnostic PCR was used with primer 1 (Int primer) and primer 3 (ol492) to  
723 confirm integration of the GFP targeting construct (**Fig S1B**). A list of primers used to  
724 amplify these genes can be found in **Table S2**.

725 The gene-deletion targeting vectors for kinesin genes were constructed using the  
726 pBS-DHFR plasmid, which contains polylinker sites flanking a *Toxoplasma gondii dhfr/ts*  
727 expression cassette conferring resistance to pyrimethamine, as described previously  
728 (Tewari et al., 2010). The 5' upstream sequences from genomic DNA of kinesin genes  
729 were amplified and inserted into *Apal* and *HindIII* restriction sites upstream of  
730 the *dhfr/ts* cassette of pBS-DHFR. The DNA fragments amplified from the 3' flanking  
731 region of kinesin genes were then inserted downstream of the *dhfr/ts* cassette using  
732 *EcoRI* and *XbaI* restriction sites. The linear targeting sequence was released using  
733 *Apal/XbaI*. A schematic representation of the endogenous *kinesin* loci, the constructs  
734 and the recombined *kinesin* loci can be found in **Fig. S3**. The primers used to generate  
735 the mutant parasite lines can be found in **Table S2**. A diagnostic PCR was used with  
736 primer 1 (Int primer) and primer 2 (ol248) to confirm integration of the targeting construct,  
737 and primer 3 (KO1) and primer 4 (KO2) were used to confirm deletion of the *kinesin*  
738 genes (**Fig. S3, Table S2**).

739 To study the function of kinesin-13, we used two conditional knock down systems;  
740 an auxin inducible degron (kinesin13AID) system and a promoter exchange/trap using  
741 double homologous recombination (kinesin-13PTD). For the generation of transgenic  
742 Kinesin-13AID/HA line, library clone PbG01-2471h08 from the PlasmogEM repository  
743 (<http://plasmogem.sanger.ac.uk/>) was used. Sequential recombineering and gateway  
744 steps were performed as previously described (Pfander et al., 2013; Pfander et al.,  
745 2011). Insertion of the GW cassette following gateway reaction was confirmed using  
746 primer pairs GW1 x *kinesin-13* QCR1 and GW2 x *kinesin-13* QCR2. The modified library  
747 inserts were then released from the plasmid backbone using NotI. The kinesin-13-  
748 AID/HA targeting vector was transfected into the 615-parasite line and conditional  
749 degradation of kinesin-13-AID/HA in the non-clonal line was performed as described  
750 previously (Balestra et al., 2020). A schematic representation of the endogenous *kinesin*-  
751 *13* locus, the constructs and the recombined *kinesin-13* locus can be found in **Fig S6A**.  
752 A diagnostic PCR was performed for *kinesin-13* gene knockdown parasites as outlined in  
753 **Fig. S6A**. Primer pairs *Kinesin-13*QCR1/GW1, and *Kinesin-13* QCR2/GW2 were used to

754 determine successful integration of the targeting construct at the 3' end of the gene (**Fig**  
755 **S6B**).

756  
757 The conditional knockdown construct kinesin-13PTD was derived from  $P_{clag}$  (pSS367)  
758 where *kinesin-13* was placed under the control of the *clag* gene (PBANKA\_083630)  
759 promoter, as described previously (Sebastian et al., 2012). A schematic representation  
760 of the endogenous *kinesin-13* locus, the constructs and the recombined *kinesin-13* locus  
761 can be found in **Fig. S6D**. A diagnostic PCR was performed for *kinesin-13* gene  
762 knockdown parasites as outlined in **Fig. S6D**. Primer 1 (5'-intPTD50) and Primer 2 (5'-  
763 intPTD) were used to determine successful integration of the targeting construct at the 5'  
764 end of the gene. Primer 3 (3'-intPTclag) and Primer 4 (3'-intPTD50) were used to  
765 determine successful integration for the 3' end of the gene locus (**Fig. S6E**). All the  
766 primer sequences can be found in **Table S2**. *P. berghei* ANKA line 2.34 (for GFP-  
767 tagging) or ANKA line 507cl1 expressing GFP (for the gene deletion and knockdown  
768 construct) parasites were transfected by electroporation (Janse et al., 2006).

### 769 **Parasite phenotype analyses**

770  
771 Blood containing approximately 50,000 parasites of the kinesin knockout/knockdown  
772 lines was injected intraperitoneally (i.p) into mice to initiate infection. Asexual stages and  
773 gametocyte production were monitored by microscopy on Giemsa-stained thin smears.  
774 Four to five days post infection, exflagellation and ookinete conversion were examined  
775 as described previously (Guttery et al., 2012) with a Zeiss AxioImager M2 microscope  
776 (Carl Zeiss, Inc) fitted with an AxioCam ICc1 digital camera. To analyse mosquito  
777 transmission, 30–50 *Anopheles stephensi* SD 500 mosquitoes were allowed to feed for  
778 20 min on anaesthetized, infected mice whose asexual parasitaemia had reached 15%  
779 and were carrying comparable numbers of gametocytes as determined on Giemsa  
780 stained blood films. To assess mid-gut infection, approximately 15 guts were dissected  
781 from mosquitoes on day-7 and -14 post feeding and oocysts were counted using a 63x  
782 oil immersion objective. On day 21 post-feeding, another 20 mosquitoes were dissected,  
783 and their guts and salivary glands crushed separately in a loosely fitting homogenizer to  
784 release sporozoites, which were then quantified using a haemocytometer or used for  
785 imaging. Mosquito bite back experiments were performed 21 days post-feeding using  
786 naive mice, and blood smears were examined after 3-4 days.

### 787 **Purification of schizonts, gametocytes and ookinetes**

788  
789 Blood cells obtained from infected mice (day 4 post infection) were cultured for 8 h and  
790 24 h at 37°C (with rotation at 100 rpm) and schizonts were purified on a 60% v/v  
791 NycoDenz (in PBS) gradient, (NycoDenz stock solution: 27.6% w/v NycoDenz in 5 mM  
792 Tris-HCl, pH 7.20, 3 mM KCl, 0.3 mM EDTA).

793 The purification of gametocytes was achieved by injecting parasites into phenylhydrazine  
794 treated mice (Beetsma et al., 1998) and enriched by sulfadiazine treatment after 2 days  
795 of infection. The blood was collected on day 4 after infection and gametocyte-infected  
796 cells were purified on a 48% v/v NycoDenz (in PBS) gradient (NycoDenz stock solution:  
797 27.6% w/v NycoDenz in 5 mM Tris-HCl, pH 7.20, 3 mM KCl, 0.3 mM EDTA). The  
798 gametocytes were harvested from the interface and activated.

799 Blood cells obtained from infected mice (day 4-5 post infection) with high gametocytemia  
800 (>20%) were cultured for 24 h in ookinete medium having xanthurenic acid at 20 °C. The  
801 ookinetes were pelleted at 1900 rpm (500 g), the supernatant was discarded, and the  
802 cells were resuspended in 8 ml ookinete medium. Five µl of magnetic beads coated with  
803 13.1 antibody (anti-P28 of ookinete) were added and incubated for 10 min at RT with

304 continuous mixing. The tubes were placed on the magnet (Dyna rack) for 2 min and  
305 supernatant was transferred into new tubes. The beads with bound ookinetes were  
306 washed with 2 ml of ookinete medium and used for imaging or electron microscopy.

### 307 308 **Live cell imaging**

309 To examine kinesin-GFP expression during erythrocyte stages, parasites growing in  
310 schizont culture medium were used for imaging at different stages (ring, trophozoite,  
311 schizont and merozoite) of development. Purified gametocytes were examined for GFP  
312 expression and cellular location at different time points (0, 1-15 min) after activation in  
313 ookinete medium (Zeeshan et al., 2019b). Zygote and ookinete stages were analyzed  
314 throughout 24 h of culture. Oocysts and sporozoites were imaged using infected  
315 mosquito guts. Images were captured using a 63x oil immersion objective on a Zeiss  
316 Axio Imager M2 microscope fitted with an AxioCam ICc1 digital camera.

### 317 318 **Generation of dual tagged parasite lines**

319 The kinesin-GFP (kinesin-5, -8X, -13 and -X4) parasites were mixed with NDC80-cherry  
320 and kinesin8B-cherry parasites in equal numbers and injected into mice. Mosquitoes  
321 were fed on mice 4 to 5 days after infection when gametocytemia was high. These  
322 mosquitoes were checked for oocyst development and sporozoite formation at day 14  
323 and day 21 after feeding. Infected mosquitoes were then allowed to feed on naïve mice  
324 and after 4 - 5 days the mice were examined for blood stage parasitaemia by microscopy  
325 with Giemsa-stained blood smears. In this way, some parasites expressed both kinesin-  
326 GFP and NDC80-cherry; and kinesin-GFP and kinesin-8B-cherry in the resultant  
327 gametocytes, and these were purified and fluorescence microscopy images were  
328 collected as described above.

### 329 330 **Ookinete and sporozoite motility assays**

331 Sporozoites were isolated from the salivary glands of mosquitoes infected with WTGFP  
332 and  $\Delta$ *kinesin-20* parasites 21 days post infection. Isolated sporozoites in RPMI 1640  
333 containing 3% bovine serum albumin (Fisher Scientific) were pelleted (5 min, 5,000 rpm,  
334 4°C) and used for motility assay. The assay using Matrigel was performed as described  
335 previously (Volkman et al., 2012; Zeeshan et al., 2020a). A small volume (20  $\mu$ l) of  
336 sporozoites, isolated as above for WT-GFP and  $\Delta$ *kinesin-20* parasites, were mixed with  
337 Matrigel (Corning). The mixture (6  $\mu$ l) was transferred onto a microscope slide with a  
338 cover slip and sealed with nail polish. After identifying a field containing sporozoites,  
339 time-lapse videos (one frame every 2 s for 100 cycles) were taken using the differential  
340 interference contrast settings with a 63x objective lens on a Zeiss AxioImager M2  
341 microscope fitted with an AxioCam ICc1 digital camera and analysed with the AxioVision  
342 4.8.2 software.

343 For ookinete motility, 24 h ookinete cultures were added to an equal volume of  
344 Matrigel on ice, mixed thoroughly, dropped onto a slide, covered with a cover slip, and  
345 sealed with nail polish. The Matrigel was then allowed to set at 20°C for 30 min. After  
346 identifying a field containing ookinetes, time-lapse videos were taken (one frame every 5  
347 s for 100 cycles).

### 348 349 **Fixed Immunofluorescence Assay**

350 The kinesin-GFP gametocytes were purified, activated in ookinete medium, fixed with  
351 4% paraformaldehyde (PFA, Sigma) diluted in microtubule stabilising buffer (MTSB) for  
352 10-15 min and added to poly-L-lysine coated slides. Immunocytochemistry was  
353 performed using primary GFP-specific rabbit monoclonal antibody (mAb) (Invitrogen-

354 A1122; used at 1:250) and primary mouse anti- $\alpha$  tubulin mAb (Sigma-T9026; used at  
355 1:1000). Secondary antibodies were Alexa 488 conjugated anti-mouse IgG (Invitrogen-  
356 A11004) and Alexa 568 conjugated anti-rabbit IgG (Invitrogen-A11034) (used at 1  
357 1000). The slides were then mounted in Vectashield 19 with DAPI (Vector Labs) for  
358 fluorescence microscopy. Parasites were visualised on a Zeiss AxioImager M2  
359 microscope fitted with an AxioCam ICc1 digital camera.

### 360 **Ultrastructure expansion microscopy (U-ExM)**

362 Purified gametocytes were activated for 4-5 min and 15 min; activation was stopped by  
363 adding 1X ice cold PBS. Activated gametocytes and mature ookinetes were sedimented  
364 onto 12 mm round Poly-D-Lysine (A3890401, Gibco) coated coverslips for 10 min  
365 (gametocyte procedure was performed on ice), fixed in  $-20^{\circ}\text{C}$  methanol for 7 min, and  
366 then prepared for U-ExM as previously described (Bertiaux et al., 2021; Gambarotto et  
367 al., 2021). Immuno-labelling was performed using primary antibody against  $\alpha$ -tubulin and  
368  $\beta$ -tubulin (1:200 dilution, source: Geneva antibody facility) and secondary antibody anti-  
369 guinea pig Alexa 488 (1:400 dilution, source: ThermoFisher). Images were acquired on a  
370 Leica TCS SP8 microscope, image analysis was performed using Fiji-Image J and Leica  
371 Application Suite X (LAS X) software.

### 372 **Electron microscopy**

374 Gametocytes activated for 6 min and 15 min and ookinetes were fixed in 4%  
375 glutaraldehyde in 0.1 M phosphate buffer and processed for electron microscopy  
376 (Ferguson et al., 2005). Briefly, samples were post fixed in osmium tetroxide, treated *en*  
377 *bloc* with uranyl acetate, dehydrated and embedded in Spurr's epoxy resin. Thin sections  
378 were stained with uranyl acetate and lead citrate prior to examination in a JEOL JEM-  
379 1400 electron microscope (JEOL Ltd, UK).

### 380 **RNA isolation and quantitative Real Time PCR (qRT-PCR) analyses**

382 RNA was isolated from purified gametocytes using an RNA purification kit (Stratagene).  
383 cDNA was synthesised using an RNA-to-cDNA kit (Applied Biosystems). Gene  
384 expression was quantified from 80 ng of total RNA using SYBR green fast master mix kit  
385 (Applied Biosystems). All the primers were designed using primer3 (Primer-blast, NCBI).  
386 Analysis was conducted using an Applied Biosystems 7500 fast machine with the  
387 following cycling conditions:  $95^{\circ}\text{C}$  for 20 s followed by 40 cycles of  $95^{\circ}\text{C}$  for 3 s;  $60^{\circ}\text{C}$  for  
388 30 s. Three technical replicates and three biological replicates were performed for each  
389 assayed gene. The *hsp70* (PBANKA\_081890) and *arginyl-t RNA synthetase*  
390 (PBANKA\_143420) genes were used as endogenous control reference genes. The  
391 primers used for qPCR can be found in **Table S2**.

### 392 **RNA-seq analysis**

394 Libraries were prepared from lyophilized total RNA, first by isolating mRNA using  
395 NEBNext Poly(A) mRNA Magnetic Isolation Module (NEB), then using NEBNext Ultra  
396 Directional RNA Library Prep Kit (NEB) according to the manufacturer's instructions.  
397 Libraries were amplified for a total of 12 PCR cycles (12 cycles of [15 s at  $98^{\circ}\text{C}$ , 30 s at  
398  $55^{\circ}\text{C}$ , 30 s at  $62^{\circ}\text{C}$ ]) using the KAPA HiFi HotStart Ready Mix (KAPA Biosystems).  
399 Libraries were sequenced using a NovaSeq 6000 DNA sequencer (Illumina), producing  
400 paired-end 100-bp reads.

401 FastQC (<https://www.bioinformatics.babraham.ac.uk/projects/fastqc/>), was used to  
402 analyse raw read quality, and based on this information, the first 11 bp of each read and  
403 any adapter sequences were removed using Trimmomatic

904 (<http://www.usadellab.org/cms/?page=trimmomatic>). Bases were trimmed from reads  
905 using Sickle with a Phred quality threshold of 25 (<https://github.com/najoshi/sickle>). The  
906 resulting reads were mapped against the *P. berghei* ANKA genome (v36) using HISAT2  
907 (version 2-2.1.0), using default parameters. Uniquely mapped, properly paired reads with  
908 mapping quality 40 or higher were retained using SAMtools  
909 (<http://samtools.sourceforge.net/>). Genome browser tracks were generated and viewed  
910 using the Integrative Genomic Viewer (IGV) (Broad Institute). Raw read counts were  
911 determined for each gene in the *P. berghei* genome using BedTools  
912 (<https://bedtools.readthedocs.io/en/latest/#>) to intersect the aligned reads with the  
913 genome annotation. Differential expression analysis was done by use of R package  
914 DESeq2 to call up- and down-regulated genes with an adjusted P-value cutoff of 0.05.  
915 Gene ontology enrichment was done using R package topGO  
916 (<https://bioconductor.org/packages/release/bioc/html/topGO.html>) with the weight01  
917 algorithm.

### 918 **ChIP-seq analysis**

919 Gametocytes for kinesin-5GFP and kinesin-8XGFP parasites were harvested and the  
920 pellets were resuspended in 500  $\mu$ l of Hi-C lysis buffer (25 mM Tris-HCl, pH 8.0, 10 mM  
921 NaCl, 2 mM AESBF, 1% NP-40, protease inhibitors). After incubation for 10 min at room  
922 temperature (RT), the resuspended pellets were homogenized by passing through a 26.5  
923 gauge needle/syringe 15 times and cross-linked by adding formaldehyde (1.25% final  
924 concentration) for 25 min at RT with continuous mixing. Crosslinking was stopped by  
925 adding glycine to a final concentration of 150 mM and incubating for 15 min at RT with  
926 continuous mixing. The sample was centrifuged for 5 min at 2,500 x g (~5,000 rpm) at  
927 4°C, the pellet washed once with 500  $\mu$ l ice-cold wash buffer (50 mM Tris-HCl, pH 8.0,  
928 50 mM NaCl, 1 mM EDTA, 2 mM AESBF, protease inhibitors) and the pellet stored at -  
929 80°C for ChIP seq analysis. The crosslinked parasite pellets were resuspended in 1 mL  
930 of nuclear extraction buffer (10 mM HEPES, 10 mM KCl, 0.1 mM EDTA, 0.1 mM EGTA,  
931 1 mM DTT, 0.5 mM AEBSEF, 1X protease inhibitor tablet), post 30 min incubation on ice,  
932 0.25% Igepal-CA-630 was added and homogenized by passing through a 26G x 1/2  
933 needle. The nuclear pellet extracted through 5000 rpm centrifugation, was resuspended  
934 in 130  $\mu$ l of shearing buffer (0.1% SDS, 1 mM EDTA, 10 mM Tris-HCl pH 7.5, 1X  
935 protease inhibitor tablet), and transferred to a 130  $\mu$ l Covaris sonication microtube. The  
936 sample was then sonicated using a Covaris S220 Ultrasonicator for 8 min (Duty cycle:  
937 5%, Intensity peak power: 140, Cycles per burst: 200, Bath temperature: 6°C). The  
938 sample was transferred to ChIP dilution buffer (30 mM Tris-HCl pH 8, 3 mM EDTA, 0.1%  
939 SDS, 30 mM NaCl, 1.8% Triton X-100, 1X protease inhibitor tablet, 1X phosphatase  
940 inhibitor tablet) and centrifuged for 10 min at 13,000 rpm at 4°C, retaining the  
941 supernatant. For each sample, 13  $\mu$ l of protein A agarose/salmon sperm DNA beads  
942 were washed three times with 500  $\mu$ l ChIP dilution buffer (without inhibitors) by  
943 centrifuging for 1 min at 1000 rpm at room temperature, then buffer was removed. For  
944 pre-clearing, the diluted chromatin samples were added to the beads and incubated for 1  
945 hour at 4°C with rotation, then pelleted by centrifugation for 1 min at 1000 rpm.  
946 Supernatant was removed into a LoBind tube carefully so as not to remove any beads  
947 and 2  $\mu$ g of anti-GFP antibody (Abcam ab290, anti-rabbit) were added to the sample and  
948 incubated overnight at 4°C with rotation. Per sample, 25  $\mu$ l of protein A agarose/salmon  
949 sperm DNA beads were washed with ChIP dilution buffer (no inhibitors), blocked with 1  
950 mg/mL BSA for 1 hour at 4°C, then washed three more times with buffer. 25  $\mu$ l of  
951 washed and blocked beads were added to the sample and incubated for 1 hour at 4°C  
952 with continuous mixing to collect the antibody/protein complex. Beads were pelleted by  
953

centrifugation for 1 min at 1000 rpm at 4°C. The bead/antibody/protein complex was then washed with rotation using 1 mL of each buffers twice; low salt immune complex wash buffer (1% SDS, 1% Triton X-100, 2 mM EDTA, 20 mM Tris-HCl pH 8, 150 mM NaCl), high salt immune complex wash buffer (1% SDS, 1% Triton X-100, 2 mM EDTA, 20 mM Tris-HCl pH 8, 500 mM NaCl), high salt immune complex wash buffer (1% SDS, 1% Triton X-100, 2 mM EDTA, 20 mM Tris-HCl pH 8, 500 mM NaCl), TE wash buffer (10 mM Tris-HCl pH 8, 1 mM EDTA) and eluted from antibody by adding 250 µl of freshly prepared elution buffer (1% SDS, 0.1 M sodium bicarbonate). We added 5 M NaCl to the elution and cross-linking was reversed by heating at 45°C overnight followed by addition of 15 µl of 20 mg/mL RNAase A with 30 min incubation at 37°C. After this, 10 µl 0.5 M EDTA, 20 µl 1 M Tris-HCl pH 7.5, and 2 µl 20 mg/mL proteinase K were added to the elution and incubated for 2 hours at 45°C. DNA was recovered by phenol/chloroform extraction and ethanol precipitation, using a phenol/chloroform/isoamyl alcohol (25:24:1) mixture twice and chloroform once, then adding 1/10 volume of 3 M sodium acetate pH 5.2, 2 volumes of 100% ethanol, and 1/1000 volume of 20 mg/mL glycogen. Precipitation was allowed to occur overnight at -20°C. Samples were centrifuged at 13,000 rpm for 30 min at 4°C, then washed with fresh 80% ethanol, and centrifuged again for 15 min with the same settings. Pellet was air-dried and resuspended in 50 µl nuclease-free water. DNA was purified using Agencourt AMPure XP beads. Libraries were then prepared from this DNA using a KAPA library preparation kit (KK8230), and sequenced on a NovaSeq 6000 machine. FastQC (<https://www.bioinformatics.babraham.ac.uk/projects/fastqc/>), was used to analyze raw read quality. Any adapter sequences were removed using Trimmomatic (<http://www.usadellab.org/cms/?page=trimmomatic>). Bases with Phred quality scores below 25 were trimmed using Sickle (<https://github.com/najoshi/sickle>). The resulting reads were mapped against the *P. berghei* ANKA genome (v36) using Bowtie2 (version 2.3.4.1). Using Samtools, only properly paired reads with mapping quality 40 or higher were retained, and reads marked as PCR duplicates were removed by PicardTools MarkDuplicates (Broad Institute). Genome browser tracks were generated and viewed using the Integrative Genomic Viewer (IGV).

### Statistical analysis

All statistical analyses were performed using GraphPad Prism 7 (GraphPad Software). For qRT-PCR, an unpaired t-test was used to examine significant differences between wild-type and mutant strains.

### Acknowledgments

We wish to thank Julie Rodgers for helping to maintain the insectary and other technical works.

**Funding:** This work was supported by: MRC UK (G0900109, G0900278, MR/K011782/1) and BBSRC (BB/N017609/1) to RT; the BBSRC (BB/N017609/1) to MZ; the Francis Crick Institute, the Cancer Research UK (FC001097), the UK Medical Research Council (FC001097), and the Wellcome Trust (FC001097) to AAH; the NIH/NIAID (R01 AI136511) and the University of California, Riverside (NIFA-Hatch-225935) to KGLR; the Swiss National Science Foundation project grant (31003A\_179321) to MB and BBSRC (BB/N018176/1) to CAM. This research was funded in whole, or in part, by the Wellcome Trust [FC001097]. For

003 the purpose of Open Access, the author has applied a CC BY public copyright  
004 licence to any Author Accepted Manuscript version arising from this submission.  
005

### 006 **Author contributions:**

007 Conceptualization: RT

008 Methodology: MZ, DB, RT, RR, SA, ZC, DJPF

009 Investigation: MZ, DB, RT, RR, SA, ZC, DJPF

010 Visualization: MZ, RT, RR, SA, DJPF

011 Supervision: RT, AAH, KGLR, CAM, MB

012 Writing—original draft: RT, MZ

013 Writing—review & editing: RT, MZ, AAH, KGLR, CAM, MB, DJPF  
014

015 **Competing interests:** All other authors declare they have no competing interests.  
016

017 **Data and materials availability:** Sequence reads for ChIP-seq and RNA-seq have been  
018 deposited in the NCBI Sequence Read Archive with accession number: PRJNA731497.  
019 All other data are available in the main text or the supplementary materials.  
020

### 021 **References**

- 022 .
- 023 Ali, A., S.N. Veeranki, A. Chinchole, and S. Tyagi. 2017. MLL/WDR5 Complex Regulates  
024 Kif2A Localization to Ensure Chromosome Congression and Proper Spindle  
025 Assembly during Mitosis. *Dev Cell.* 41:605-622 e607.
- 026 Andreadaki, M., T. Pace, F. Grasso, I. Siden-Kiamos, S. Mochi, L. Picci, L. Bertuccini, M.  
027 Ponzi, and C. Curra. 2020. Plasmodium berghei Gamete Egress Protein is  
028 required for fertility of both genders. *Microbiologyopen.* 9:e1038.
- 029 Balestra, A.C., M. Zeeshan, E. Rea, C. Pasquarello, L. Brusini, T. Mourier, A.K. Subudhi,  
030 N. Klages, P. Arboit, R. Pandey, D. Brady, S. Vaughan, A.A. Holder, A. Pain, D.J.  
031 Ferguson, A. Hainard, R. Tewari, and M. Brochet. 2020. A divergent cyclin/cyclin-  
032 dependent kinase complex controls the atypical replication of a malaria parasite  
033 during gametogony and transmission. *Elife.* 9.
- 034 Beetsma, A.L., T.J. van de Wiel, R.W. Sauerwein, and W.M. Eling. 1998. Plasmodium  
035 berghei ANKA: purification of large numbers of infectious gametocytes. *Exp*  
036 *Parasitol.* 88:69-72.
- 037 Bertiaux, E., A.C. Balestra, L. Bournonville, V. Louvel, B. Maco, D. Soldati-Favre, M.  
038 Brochet, P. Guichard, and V. Hamel. 2021. Expansion microscopy provides new  
039 insights into the cytoskeleton of malaria parasites including the conservation of a  
040 conoid. *PLoS Biol.* 19:e3001020.
- 041 Billker, O., V. Lindo, M. Panico, A.E. Etienne, T. Paxton, A. Dell, M. Rogers, R.E. Sinden,  
042 and H.R. Morris. 1998. Identification of xanthurenic acid as the putative inducer of  
043 malaria development in the mosquito. *Nature.* 392:289-292.
- 044 Briggs, L.J., J.A. Davidge, B. Wickstead, M.L. Ginger, and K. Gull. 2004. More than one  
045 way to build a flagellum: comparative genomics of parasitic protozoa. *Curr Biol.*  
046 14:R611-612.
- 047 Bushell, E., A.R. Gomes, T. Sanderson, B. Anar, G. Girling, C. Herd, T. Metcalf, K.  
048 Modrzynska, F. Schwach, R.E. Martin, M.W. Mather, G.I. McFadden, L. Parts,  
049 G.G. Rutledge, A.B. Vaidya, K. Wengelnik, J.C. Rayner, and O. Billker. 2017.  
050 Functional Profiling of a Plasmodium Genome Reveals an Abundance of  
051 Essential Genes. *Cell.* 170:260-272 e268.

- 052 Chan, K.Y., and K. Ersfeld. 2010. The role of the Kinesin-13 family protein TbKif13-2 in  
053 flagellar length control of *Trypanosoma brucei*. *Mol Biochem Parasitol.* 174:137-  
054 140.
- 055 Dawson, S.C., M.S. Sagolla, J.J. Mancuso, D.J. Woessner, S.A. House, L. Fritz-Laylin,  
056 and W.Z. Cande. 2007. Kinesin-13 regulates flagellar, interphase, and mitotic  
057 microtubule dynamics in *Giardia intestinalis*. *Eukaryot Cell.* 6:2354-2364.
- 058 Depoix, D., S.R. Marques, D.J. Ferguson, S. Chaouch, T. Duguet, R.E. Sinden, P.  
059 Grellier, and L. Kohl. 2020. Vital role for *Plasmodium berghei* Kinesin8B in  
060 axoneme assembly during male gamete formation and mosquito transmission.  
061 *Cell Microbiol.* 22:e13121.
- 062 Ems-McClung, S.C., and C.E. Walczak. 2010. Kinesin-13s in mitosis: Key players in the  
063 spatial and temporal organization of spindle microtubules. *Semin Cell Dev Biol.*  
064 21:276-282.
- 065 Fang, H., N. Klages, B. Baechler, E. Hillner, L. Yu, M. Pardo, J. Choudhary, and M.  
066 Brochet. 2017. Multiple short windows of calcium-dependent protein kinase 4  
067 activity coordinate distinct cell cycle events during *Plasmodium* gametogenesis.  
068 *Elife.* 6.
- 069 Ferguson, D.J., F.L. Henriquez, M.J. Kirisits, S.P. Muench, S.T. Prigge, D.W. Rice, C.W.  
070 Roberts, and R.L. McLeod. 2005. Maternal inheritance and stage-specific  
071 variation of the apicoplast in *Toxoplasma gondii* during development in the  
072 intermediate and definitive host. *Eukaryot Cell.* 4:814-826.
- 073 Gambarotto, D., V. Hamel, and P. Guichard. 2021. Ultrastructure expansion microscopy  
074 (U-ExM). *Methods Cell Biol.* 161:57-81.
- 075 Gao, H., Z. Yang, X. Wang, P. Qian, R. Hong, X. Chen, X.Z. Su, H. Cui, and J. Yuan.  
076 2018. ISP1-Anchored Polarization of GCbeta/CDC50A Complex Initiates Malaria  
077 Ookinete Gliding Motility. *Curr Biol.* 28:2763-2776 e2766.
- 078 Gould, S.B., W.H. Tham, A.F. Cowman, G.I. McFadden, and R.F. Waller. 2008.  
079 Alveolins, a new family of cortical proteins that define the protist infrakingdom  
080 Alveolata. *Mol Biol Evol.* 25:1219-1230.
- 081 Graumans, W., E. Jacobs, T. Bousema, and P. Sinnis. 2020. When Is a Plasmodium-  
082 Infected Mosquito an Infectious Mosquito? *Trends Parasitol.* 36:705-716.
- 083 Gubbels, M.J., C.D. Keroack, S. Dangoudoubiyam, H.L. Worliczek, A.S. Paul, C.  
084 Bauwens, B. Elsworth, K. Engelberg, D.K. Howe, I. Coppens, and M.T.  
085 Duraisingh. 2020. Fussing About Fission: Defining Variety Among Mainstream  
086 and Exotic Apicomplexan Cell Division Modes. *Front Cell Infect Microbiol.* 10:269.
- 087 Guttery, D.S., B. Poulin, D.J. Ferguson, B. Szoor, B. Wickstead, P.L. Carroll, C.  
088 Ramakrishnan, D. Brady, E.M. Patzewitz, U. Straschil, L. Solyakov, J.L. Green,  
089 R.E. Sinden, A.B. Tobin, A.A. Holder, and R. Tewari. 2012. A unique protein  
090 phosphatase with kelch-like domains (PPKL) in *Plasmodium* modulates ookinete  
091 differentiation, motility and invasion. *PLoS Pathog.* 8:e1002948.
- 092 Hammarton, T.C. 2019. Who Needs a Contractile Actomyosin Ring? The Plethora of  
093 Alternative Ways to Divide a Protozoan Parasite. *Front Cell Infect Microbiol.*  
094 9:397.
- 095 Hirokawa, N., and Y. Tanaka. 2015. Kinesin superfamily proteins (KIFs): Various  
096 functions and their relevance for important phenomena in life and diseases. *Exp*  
097 *Cell Res.* 334:16-25.
- 098 Invergo, B.M., M. Brochet, L. Yu, J. Choudhary, P. Beltrao, and O. Billker. 2017. Sub-  
099 minute Phosphoregulation of Cell Cycle Systems during *Plasmodium* Gamete  
100 Formation. *Cell Rep.* 21:2017-2029.



- 101 Iwanaga, S., T. Kato, I. Kaneko, and M. Yuda. 2012. Centromere plasmid: a new genetic  
102 tool for the study of *Plasmodium falciparum*. *PLoS One*. 7:e33326.
- 103 Janse, C.J., B. Franke-Fayard, G.R. Mair, J. Ramesar, C. Thiel, S. Engelmann, K.  
104 Matuschewski, G.J. van Gemert, R.W. Sauerwein, and A.P. Waters. 2006. High  
105 efficiency transfection of *Plasmodium berghei* facilitates novel selection  
106 procedures. *Molecular and biochemical parasitology*. 145:60-70.
- 107 Janse, C.J., B. Mons, R.J. Rouwenhorst, P.F. Van der Klooster, J.P. Overdulve, and H.J.  
108 Van der Kaay. 1985. In vitro formation of ookinetes and functional maturity of  
109 *Plasmodium berghei* gametocytes. *Parasitology*. 91 ( Pt 1):19-29.
- 110 Konjikusic, M.J., R.S. Gray, and J.B. Wallingford. 2021. The developmental biology of  
111 kinesins. *Dev Biol*. 469:26-36.
- 112 Kono, M., D. Prusty, J. Parkinson, and T.W. Gilberger. 2013. The apicomplexan inner  
113 membrane complex. *Front Biosci (Landmark Ed)*. 18:982-992.
- 114 Koreny, L., M. Zeeshan, K. Barylyuk, E.C. Tromer, J.J.E. van Hooff, D. Brady, H. Ke, S.  
115 Chelaghma, D.J.P. Ferguson, L. Eme, R. Tewari, and R.F. Waller. 2021.  
116 Molecular characterization of the conoid complex in *Toxoplasma* reveals its  
117 conservation in all apicomplexans, including *Plasmodium* species. *PLoS Biol*.  
118 19:e3001081.
- 119 Mair, G.R., J.A. Braks, L.S. Garver, J.C. Wiegant, N. Hall, R.W. Dirks, S.M. Khan, G.  
120 Dimopoulos, C.J. Janse, and A.P. Waters. 2006. Regulation of sexual  
121 development of *Plasmodium* by translational repression. *Science*. 313:667-669.
- 122 Mangione, M.C., and K.L. Gould. 2019. Molecular form and function of the cytokinetic  
123 ring. *J Cell Sci*. 132.
- 124 Manning, A.L., N.J. Ganem, S.F. Bakhoun, M. Wagenbach, L. Wordeman, and D.A.  
125 Compton. 2007. The kinesin-13 proteins Kif2a, Kif2b, and Kif2c/MCAK have  
126 distinct roles during mitosis in human cells. *Mol Biol Cell*. 18:2970-2979.
- 127 Marques, S.R., C. Ramakrishnan, R. Carzaniga, A.M. Blagborough, M.J. Delves, A.M.  
128 Talman, and R.E. Sinden. 2015. An essential role of the basal body protein SAS-6  
129 in *Plasmodium* male gamete development and malaria transmission. *Cell*  
130 *Microbiol*. 17:191-206.
- 131 Mirvis, M., T. Stearns, and W. James Nelson. 2018. Cilium structure, assembly, and  
132 disassembly regulated by the cytoskeleton. *Biochem J*. 475:2329-2353.
- 133 Moon, R.W., C.J. Taylor, C. Bex, R. Schepers, D. Goulding, C.J. Janse, A.P. Waters,  
134 D.A. Baker, and O. Billker. 2009. A cyclic GMP signalling module that regulates  
135 gliding motility in a malaria parasite. *PLoS Pathog*. 5:e1000599.
- 136 Moores, C.A., M. Yu, J. Guo, C. Beraud, R. Sakowicz, and R.A. Milligan. 2002. A  
137 mechanism for microtubule depolymerization by KinI kinesins. *Mol Cell*. 9:903-  
138 909.
- 139 Morano, A.A., and J.D. Dvorin. 2021. The Ringleaders: Understanding the Apicomplexan  
140 Basal Complex Through Comparison to Established Contractile Ring Systems.  
141 *Front Cell Infect Microbiol*. 11:656976.
- 142 Morrissette, N.S., and L.D. Sibley. 2002. Cytoskeleton of apicomplexan parasites.  
143 *Microbiol Mol Biol Rev*. 66:21-38; table of contents.
- 144 Okamoto, N., T.P. Spurck, C.D. Goodman, and G.I. McFadden. 2009. Apicoplast and  
145 mitochondrion in gametocytogenesis of *Plasmodium falciparum*. *Eukaryot Cell*.  
146 8:128-132.
- 147 Pandey, R., S. Abel, M. Boucher, R.J. Wall, M. Zeeshan, E. Rea, A. Freville, X.M. Lu, D.  
148 Brady, E. Daniel, R.R. Stanway, S. Wheatley, G. Batugedara, T. Hollin, A.R.  
149 Bottrill, D. Gupta, A.A. Holder, K.G. Le Roch, and R. Tewari. 2020. *Plasmodium*  
150 Condensin Core Subunits SMC2/SMC4 Mediate Atypical Mitosis and Are

- 151 Essential for Parasite Proliferation and Transmission. *Cell Rep.* 30:1883-1897  
152 e1886.
- 153 Pfander, C., B. Anar, M. Brochet, J.C. Rayner, and O. Billker. 2013. Recombination-  
154 mediated genetic engineering of *Plasmodium berghei* DNA. *Methods Mol Biol.*  
155 923:127-138.
- 156 Pfander, C., B. Anar, F. Schwach, T.D. Otto, M. Brochet, K. Volkmann, M.A. Quail, A.  
157 Pain, B. Rosen, W. Skarnes, J.C. Rayner, and O. Billker. 2011. A scalable  
158 pipeline for highly effective genetic modification of a malaria parasite. *Nat*  
159 *Methods.* 8:1078-1082.
- 160 Philip, N., and A.P. Waters. 2015. Conditional Degradation of *Plasmodium* Calcineurin  
161 Reveals Functions in Parasite Colonization of both Host and Vector. *Cell Host*  
162 *Microbe.* 18:122-131.
- 163 Piao, T., M. Luo, L. Wang, Y. Guo, D. Li, P. Li, W.J. Snell, and J. Pan. 2009. A  
164 microtubule depolymerizing kinesin functions during both flagellar disassembly  
165 and flagellar assembly in *Chlamydomonas*. *Proc Natl Acad Sci U S A.* 106:4713-  
166 4718.
- 167 Reid, A.J., A.M. Talman, H.M. Bennett, A.R. Gomes, M.J. Sanders, C.J.R. Illingworth, O.  
168 Billker, M. Berriman, and M.K. Lawniczak. 2018. Single-cell RNA-seq reveals  
169 hidden transcriptional variation in malaria parasites. *Elife.* 7.
- 170 Schrevel, J., G. Asfaux-Foucher, and J.M. Bafort. 1977. [Ultrastructural study of multiple  
171 mitoses during sporogony of *Plasmodium b. berghei*]. *J Ultrastruct Res.* 59:332-  
172 350.
- 173 Sebastian, S., M. Brochet, M.O. Collins, F. Schwach, M.L. Jones, D. Goulding, J.C.  
174 Rayner, J.S. Choudhary, and O. Billker. 2012. A *Plasmodium* calcium-dependent  
175 protein kinase controls zygote development and transmission by translationally  
176 activating repressed mRNAs. *Cell Host Microbe.* 12:9-19.
- 177 Sehring, I.M., B. Dong, E. Denker, P. Bhattachan, W. Deng, B.T. Mathiesen, and D.  
178 Jiang. 2014. An equatorial contractile mechanism drives cell elongation but not  
179 cell division. *PLoS Biol.* 12:e1001781.
- 180 Sinden, R.E. 1991. Mitosis and meiosis in malarial parasites. *Acta Leiden.* 60:19-27.
- 181 Sinden, R.E., E.U. Canning, R.S. Bray, and M.E. Smalley. 1978. Gametocyte and  
182 gamete development in *Plasmodium falciparum*. *Proc R Soc Lond B Biol Sci.*  
183 201:375-399.
- 184 Sinden, R.E., and K. Strong. 1978. An ultrastructural study of the sporogonic  
185 development of *Plasmodium falciparum* in *Anopheles gambiae*. *Trans R Soc Trop*  
186 *Med Hyg.* 72:477-491.
- 187 Sinden, R.E., A. Talman, S.R. Marques, M.N. Wass, and M.J. Sternberg. 2010. The  
188 flagellum in malarial parasites. *Curr Opin Microbiol.* 13:491-500.
- 189 Spreng, B., H. Fleckenstein, P. Kubler, C. Di Biagio, M. Benz, P. Patra, U.S. Schwarz, M.  
190 Cyrklaff, and F. Frischknecht. 2019. Microtubule number and length determine  
191 cellular shape and function in *Plasmodium*. *EMBO J.* 38:e100984.
- 192 Straschil, U., A.M. Talman, D.J. Ferguson, K.A. Bunting, Z. Xu, E. Bailes, R.E. Sinden,  
193 A.A. Holder, E.F. Smith, J.C. Coates, and T. Rita. 2010. The Armadillo repeat  
194 protein PF16 is essential for flagellar structure and function in *Plasmodium* male  
195 gametes. *PLoS One.* 5:e12901.
- 196 Talman, A.M., J.H. Prieto, S. Marques, C. Ubaida-Mohien, M. Lawniczak, M.N. Wass, T.  
197 Xu, R. Frank, A. Ecker, R.S. Stanway, S. Krishna, M.J. Sternberg, G.K.  
198 Christophides, D.R. Graham, R.R. Dinglasan, J.R. Yates, 3rd, and R.E. Sinden.  
199 2014. Proteomic analysis of the *Plasmodium* male gamete reveals the key role for  
200 glycolysis in flagellar motility. *Malar J.* 13:315.

- 201 Tewari, R., D. Dorin, R. Moon, C. Doerig, and O. Billker. 2005. An atypical mitogen-  
202 activated protein kinase controls cytokinesis and flagellar motility during male  
203 gamete formation in a malaria parasite. *Mol Microbiol.* 58:1253-1263.
- 204 Tewari, R., U. Straschil, A. Bateman, U. Bohme, I. Cherevach, P. Gong, A. Pain, and O.  
205 Billker. 2010. The systematic functional analysis of Plasmodium protein kinases  
206 identifies essential regulators of mosquito transmission. *Cell Host Microbe.* 8:377-  
207 387.
- 208 Tremp, A.Z., E.I. Khater, and J.T. Dessens. 2008. IMC1b is a putative membrane  
209 skeleton protein involved in cell shape, mechanical strength, motility, and  
210 infectivity of malaria ookinetes. *J Biol Chem.* 283:27604-27611.
- 211 Vasudevan, K.K., Y.Y. Jiang, K.F. Lechtreck, Y. Kushida, L.M. Alford, W.S. Sale, T.  
212 Hennessey, and J. Gaertig. 2015. Kinesin-13 regulates the quantity and quality of  
213 tubulin inside cilia. *Mol Biol Cell.* 26:478-494.
- 214 Vavylonis, D., J.Q. Wu, S. Hao, B. O'Shaughnessy, and T.D. Pollard. 2008. Assembly  
215 mechanism of the contractile ring for cytokinesis by fission yeast. *Science.*  
216 319:97-100.
- 217 Verhey, K.J., and J.W. Hammond. 2009. Traffic control: regulation of kinesin motors. *Nat*  
218 *Rev Mol Cell Biol.* 10:765-777.
- 219 Vicente, J.J., and L. Wordeman. 2015. Mitosis, microtubule dynamics and the evolution  
220 of kinesins. *Exp Cell Res.* 334:61-69.
- 221 Volkmann, K., C. Pfander, C. Burstroem, M. Ahras, D. Goulding, J.C. Rayner, F.  
222 Frischknecht, O. Billker, and M. Brochet. 2012. The alveolin IMC1h is required for  
223 normal ookinete and sporozoite motility behaviour and host colonisation in  
224 Plasmodium berghei. *PLoS One.* 7:e41409.
- 225 Wall, R.J., M. Zeeshan, N.J. Katris, R. Limenitakis, E. Rea, J. Stock, D. Brady, R.F.  
226 Waller, A.A. Holder, and R. Tewari. 2019. Systematic analysis of Plasmodium  
227 myosins reveals differential expression, localisation, and function in invasive and  
228 proliferative parasite stages. *Cell Microbiol.* 21:e13082.
- 229 Wang, X., P. Qian, H. Cui, L. Yao, and J. Yuan. 2020. A protein palmitoylation cascade  
230 regulates microtubule cytoskeleton integrity in Plasmodium. *EMBO J.*  
231 39:e104168.
- 232 Wickstead, B., and K. Gull. 2006. A "holistic" kinesin phylogeny reveals new kinesin  
233 families and predicts protein functions. *Mol Biol Cell.* 17:1734-1743.
- 234 Wickstead, B., and K. Gull. 2011. The evolution of the cytoskeleton. *J Cell Biol.* 194:513-  
235 525.
- 236 Wickstead, B., K. Gull, and T.A. Richards. 2010. Patterns of kinesin evolution reveal a  
237 complex ancestral eukaryote with a multifunctional cytoskeleton. *BMC Evol Biol.*  
238 10:110.
- 239 Yount, A.L., H. Zong, and C.E. Walczak. 2015. Regulatory mechanisms that control  
240 mitotic kinesins. *Exp Cell Res.* 334:70-77.
- 241 Zeeshan, M., D. Brady, R.R. Stanway, C.A. Moores, A.A. Holder, and R. Tewari. 2020a.  
242 Plasmodium berghei Kinesin-5 Associates With the Spindle Apparatus During Cell  
243 Division and Is Important for Efficient Production of Infectious Sporozoites. *Front*  
244 *Cell Infect Microbiol.* 10:583812.
- 245 Zeeshan, M., D.J. Ferguson, S. Abel, A. Burrell, E. Rea, D. Brady, E. Daniel, M. Delves,  
246 S. Vaughan, A.A. Holder, K.G. Le Roch, C.A. Moores, and R. Tewari. 2019a.  
247 Kinesin-8B controls basal body function and flagellum formation and is key to  
248 malaria transmission. *Life Sci Alliance.* 2.
- 249 Zeeshan, M., R. Pandey, D.J.P. Ferguson, E.C. Tromer, R. Markus, S. Abel, D. Brady,  
250 E. Daniel, R. Limenitakis, A.R. Bottrill, K.G. Le Roch, A.A. Holder, R.F. Waller,

251 D.S. Guttery, and R. Tewari. 2020b. Real-time dynamics of Plasmodium NDC80  
252 reveals unusual modes of chromosome segregation during parasite proliferation.  
253 *J Cell Sci.* 134.

254 Zeeshan, M., R. Pandey, A.K. Subudhi, D.J.P. Ferguson, G. Kaur, R. Rashpa, R.  
255 Nugmanova, D. Brady, A.R. Bottrill, S. Vaughan, M. Brochet, M. Bollen, A. Pain,  
256 A.A. Holder, D.S. Guttery, and R. Tewari. 2021. Protein Phosphatase 1 regulates  
257 atypical mitotic and meiotic division in Plasmodium sexual stages. *bioRxiv*.

258 Zeeshan, M., F. Shilliday, T. Liu, S. Abel, T. Mourier, D.J.P. Ferguson, E. Rea, R.R.  
259 Stanway, M. Roques, D. Williams, E. Daniel, D. Brady, A.J. Roberts, A.A. Holder,  
260 A. Pain, K.G. Le Roch, C.A. Moores, and R. Tewari. 2019b. Plasmodium kinesin-  
261 8X associates with mitotic spindles and is essential for oocyst development during  
262 parasite proliferation and transmission. *PLoS Pathog.* 15:e1008048.

## 263 264 265 **Figure legends**

266  
267 **Fig 1. Kinesin pattern of expression and diverse subcellular locations at various**  
268 **stages in the *Plasmodium berghei* life cycle. (A)** Life cycle of *Plasmodium spp.*  
269 Showing different proliferative and invasive stages in its host and vector. **(B)** A summary  
270 of expression and location of kinesins-GFP during different stages of *P. berghei* life  
271 cycle. **(C)** Live cell imaging showing subcellular locations of nine kinesin-GFP proteins  
272 (green) during various stages of the *P. berghei* life cycle. DNA is stained with Hoechst  
273 dye (blue). Arrowhead indicates basal end and arrow indicates apical end of the  
274 ookinete. Mpa = min post activation. Oocyst-NS: non-sporulating oocyst, Oocyst-S:  
275 sporulating oocyst. Scale bar = 5  $\mu$ m.

276  
277 **Fig 2. Nuclear kinesins (kinesin-5 and -8X) associate with kinetochore and bind to**  
278 **the centromere during male gamete formation. (A)** Live cell imaging showing the  
279 temporal dynamics of kinesin-5GFP (green) along with kinetochore marker  
280 NDC80Cherry (red) during male gametogenesis. **(B)** Live cell imaging showing the  
281 dynamics of kinesin-8XGFP (green) along with kinetochore marker NDC80Cherry (red)  
282 during male gametogenesis. **(C)** ChIP-seq analysis of kinesin-5 and kinesin-8X during  
283 gametocyte stage. Lines on top are division points between chromosomes and circles on  
284 the bottom indicate locations of centromeres. DNA is stained with Hoechst dye (blue);  
285 mpa=min post activation; Scale bar=5  $\mu$ m.

286  
287 **Fig 3. Apicomplexa-enriched kinesins (kinesin-X3 and -X4) are located at the**  
288 **pellicle during ookinete differentiation and axonemes in male gametogenesis,**  
289 **respectively. (A)** Live cell imaging showing temporal location of kinesin-X3 (green)  
290 associated with pellicle formation (arrows) during zygote to ookinete transition (2-24 h). A  
291 cy3-conjugated antibody, 13.1, which recognises the protein P28 on the surface of  
292 zygote and ookinete stages, was used to track these stages (red). DNA is stained with  
293 Hoechst dye (blue). Scale bar=5  $\mu$ m. **(B)** Live cell imaging shows the association of  
294 kinesin-X4 (green) with axoneme marker kinesin-8B (red) during male gametogenesis.  
295 Note in later stages, axonemes (arrows) are labelled with both markers. DNA is stained  
296 with Hoechst dye (blue). mpa = min post activation. Scale bar = 5  $\mu$ m.

297  
298 **Fig 4. Phenotypic screen of nine kinesins in Plasmodium reveals their role during**  
299 **sexual and transmission stages within mosquito vector. (A)** Summary of  
300 phenotypes at various stages of life cycle resulting from gene deletion. The phenotype

301 was examined for asexual blood stage development (schizogony), exflagellation (male  
302 gamete formation), ookinete formation, oocyst number, oocyst size, sporozoite formation  
303 in oocyst, presence of salivary gland sporozoites and sporozoite transmission to  
304 vertebrate host. N/D=Not Determined **(B)** Male gametogenesis in kinesin gene-deletion  
305 lines in comparison with WTGFP parasite, measured as the number of exflagellation  
306 centres per field; more than 20 fields were counted for each line. Mean  $\pm$  SEM. n = 3  
307 independent experiments. **(C)** Percentage ookinete conversion comparing knockout and  
308 WTGFP parasites. Ookinetes were identified using 13.1 antibody for surface marker  
309 (P28, red) and defined as those cells that differentiated successfully into elongated  
310 'banana shaped' ookinetes. Mean  $\pm$  SEM. n = 5 independent experiments. **(D)** Total  
311 number of GFP-positive oocysts per mosquito midgut at 7-, 14- and 21-days post  
312 infection for knockout and WTGFP parasites; at least 10 mosquito midguts were counted  
313 for each line. Mean  $\pm$  SEM. n= 3 independent experiments. **(E)** Representative mosquito  
314 midguts at 10x and 63x magnification showing oocysts of kinesin knockout and WTGFP  
315 lines at 7-, 14- and 21-days post infection. Scale bar = 50  $\mu$ M (10x), 20  $\mu$ M (63x). **(F)**  
316 Total number of sporozoites in oocysts of kinesin knockout and WTGFP parasites at 14-  
317 and 21-days post infection. Mean  $\pm$  SEM. n = 3 independent experiments. **(G)** Total  
318 number of sporozoites in salivary glands of kinesin knockout and WT-GFP parasites.  
319 Mean  $\pm$  SEM. n = 3 independent experiments. **(H)** Mosquito bite back experiments  
320 showing no transmission of  $\Delta$ kinesin-8B and  $\Delta$ kinesin-8X parasites, while other kinesin  
321 knockout and WTGFP parasites show successful transmission from mosquito to mice.  
322 Mean  $\pm$  SEM. n = 3 independent experiments. \* $p \leq 0.05$ , \*\* $p \leq 0.01$  and \*\*\* $p \leq 0.001$ .

323  
324 **Fig 5. Kinesin-20 makes a ring like structure at the base of developing ookinete**  
325 **and is important for zygote to ookinete transformation and subsequent motility.**  
326 **(A)** Live cell imaging showing localization of kinesin-20GFP (green) in the female  
327 gametocyte, zygote and during ookinete transformation. Kinesin-20GFP accumulates at  
328 the neck of developing ookinete making a ring like structure (indicated by arrows).  
329 Labelling with P28 was used to identify the surface of activated female gametes, zygotes  
330 and ookinetes and to mark these stages (red). DNA is labelled with Hoechst dye (blue)  
331 **(B).** Ookinete developmental stages for  $\Delta$ kinesin-20 and WTGFP parasites. Ookinetes  
332 were identified using P28 and defined as those cells differentiated successfully into  
333 elongated 'banana shaped' forms. Round cells are arrested zygotes or female  
334 gametocytes, while bulbous cells did not develop to banana-shaped ookinetes for  
335  $\Delta$ kinesin-20 parasites. DNA is stained with Hoechst dye (blue). Scale bar = 5  $\mu$ m. **(C)**  
336 Ookinete conversion as a percentage of cells for  $\Delta$ kinesin-20 and WTGFP parasites after  
337 24 h. Mean  $\pm$  SEM. n = 4 independent experiments. **(D)** Representative frames from  
338 time-lapse videos of motile WTGFP ookinetes and sessile ookinetes of  $\Delta$ kinesin-20 in  
339 Matrigel. Black arrow indicates apical end of ookinete. Scale bar = 5  $\mu$ m. **(E)** Ookinete  
340 motility for WT-GFP and  $\Delta$ kinesin-20 lines in Matrigel. More than 20 ookinetes were  
341 examined for each line. Mean  $\pm$  SEM. n = 3 independent experiments. **(F)**  
342 Representative frames from time-lapse videos showing motile sporozoites of WTGFP  
343 and  $\Delta$ kinesin-20 lines. Black arrow indicates the apical end of the sporozoites. Scale bar  
344 = 5  $\mu$ m. **(G)** Sporozoite motility for WTGFP and  $\Delta$ kinesin-20 lines. More than 20  
345 sporozoites were examined for each line. Mean  $\pm$  SEM. n = 3 independent experiments.  
346 **(H)** qRT-PCR analysis of transcripts for other kinesin genes in  $\Delta$ kinesin-20 and WTGFP  
347 parasites. Mean  $\pm$  SEM. n = 3 independent experiments. Ns = not significant. **(I)** RNAseq  
348 analysis showing no transcript in  $\Delta$ kinesin-20 parasites. **(J)** Volcano plot showing  
349 differentially regulated genes in  $\Delta$ kinesin-20 gametocytes activated for 2h.

**Fig 6. Ultrastructural analysis of WTGFP and  $\Delta$ kinesin-20 ookinetes. (A)**

Representative confocal images of expanded ookinetes of WTGFP and bulbous cells of  $\Delta$ kinesin-20 lines stained for  $\alpha$ - and  $\beta$ -tubulin (magenta) showing sub-pellicle MTs. Scale bar=1  $\mu$ m (B) Electron micrographs of WTGFP (a, d, f, h) and  $\Delta$ kinesin-20 (b, c, e, g, i) ookinetes. Bars represent 1  $\mu$ m (a-c) and 100 nm (d-i).

(a) Longitudinal section of a crescentic shaped WTGFP ookinete showing the apical complex (AC) with numerous micronemes (M) in the anterior cytoplasm and a more posteriorly located crystalline body (Cr) and nucleus (N). (b) Longitudinal section through an immature  $\Delta$ kinesin-20 ookinete displaying a bulbous shape. Within the cytoplasm, the apical complex (AC) plus an irregular shaped nucleus (N) and a few irregularly arranged dense granules (DG) can be identified. (c). Longitudinal section through a more mature  $\Delta$ kinesin-20 ookinete showing a bulbous shaped cell. Within the cytoplasm the apical complex (AC), nucleus (N) and crystalline body (Cr) can be identifying but note the micronemes (M) appear to be distributed throughout the cytoplasm. (d, e) Details of longitudinal sections through the apical complex of WTGFP (d) and  $\Delta$ kinesin-20 (e) ookinetes showing similar substructures consisting of three conoidal rings (CR), an anterior polar ring 1 (P1) formed by the IMC and a second polar ring (P2) representing the initiation site for the sub-pellicular microtubules (Mt). The polar rings are separated by a collar consisting of an outer electron dense layer (cd) and an inner electron lucent layer (cl). Note the micronemes (M) with ducts (D) direct to the anterior plasmalemma. (f, g) Cross section through the periphery of the anterior complex of a WTGFP (f) and a  $\Delta$ kinesin-20 (g) parasite showing similar sub-structure consisting of the outer plasmalemma (PM) and the underlying inner membrane complex (IMC) which appears fused to the outer electron dense (cd) region of the apical collar while the more electron lucent inner region is in close contact with sub-pellicular microtubules (Mt). (h, i) Cross section of the pellicle posterior to the apical complex consisting of the outer plasmalemma and the underlying IMC. However, note that while the sub-pellicular microtubules (Mt) in the WTGFP parasite (h) are evenly spaced, those of the  $\Delta$ kinesin-20 (i) show irregular spacing and some clumping.

**Fig 7. Kinesin-13 associates with kinetochore marker, NDC80, during various proliferative stages of parasite life cycle.**

Live cell imaging showing location of kinesin-13GFP (green) with respect to kinetochore marker NDC80Cherry (red) during asexual (A, B) and sexual (C, D) proliferative stages. Asexual proliferative stages include endomitosis during blood schizogony and sporogony. Sexual stages include endomitosis during male gametogenesis and meiosis during ookinete development. Kinesin-13GFP (green) shows a diffuse distribution in the cytoplasm, together with strong foci at different stages of development that co-localise with NDC80Cherry (red). DNA is stained with Hoechst dye (blue). Scale bar = 5  $\mu$ m.

**Fig 8. Phenotypic analysis of gene expression knockdown in kinesin-13PTD transgenic line at various proliferative stages during the life cycle (A)**

qRT-PCR analysis showing down-regulation of kinesin-13 gene in *kinesin-13PTD* parasites compared to WTGFP. Mean  $\pm$  SEM, n=3 independent experiments. (B) Exflagellation centres per field at 15 min post-activation. n = 3 independent experiments (>20 fields per experiment). Error bar,  $\pm$  SEM. (C) Percentage ookinete conversion from zygote. n= 3 independent experiments (> 80 cells). Error bar,  $\pm$  SEM. (D) Oocysts at days 7, 14, and 21 post infection. n = 3 independent experiments with a minimum of 8 mosquito guts. Error bar,  $\pm$  SEM. (E) Bite back experiments reveal no transmission of *kinesin-13PTD* and successful transmission of WTGFP parasites from mosquito to mouse. Mean  $\pm$

SEM. n = 3 independent experiments. **(F)** qRT-PCR analysis of transcripts for other kinesin genes in *kinesin-13PTD* compared to WTGFP parasites. n= 3 independent experiments. Error bar,  $\pm$  SEM. **(G)** RNAseq analysis showing depletion of kinesin-13 transcript in *kinesin-13PTD* parasites. **(H)** Volcano plot showing differentially regulated genes in *kinesin-13PTD* gametocytes before activation (0 min). **(I)** Volcano plot showing differentially regulated genes in *kinesin-13PTD* gametocytes activated for 15 min. **(J)** Heat maps showing differential regulation of various genes involved in axoneme biogenesis, IMC/glideosome and chromosome dynamics. \* $p \leq 0.05$ , \*\* $p \leq 0.01$  and \*\*\* $p \leq 0.001$ .

**Fig 9. Ultrastructural analysis of WTGFP and *kinesin-13PTD* gametocytes and ookinetes.** **(A)** Representative confocal images of expanded gametocytes of WTGFP and *kinesin-13PTD* lines stained for  $\alpha$ - and  $\beta$ -tubulin (magenta) showing labelling of spindle (arrow) and axonemal MTs (arrowhead) at 4-5 min and axonemal MTs (arrowhead) at 15 min post activation. Similarly, representative confocal images of expanded ookinetes of WTGFP and *kinesin-13PTD* lines stained for  $\alpha$ - and  $\beta$ -tubulin (magenta) showing well-organised subpellicular MTs (white arrows) and apical tubulin ring (ATR, red arrows) in WTGFP ookinetes and disorganised MTs were observed in *kinesin-13PTD*. Scale bars = 1  $\mu$ m. **(B)** Electron micrographs of *P. berghei* male gametogenesis of WTGFP (**a, b, e, f, g**) and *kinesin-13PTD* (**c, d, h, i**) at 6 min (**a – d**) and 15 min (**e – i**) post-activation. Bars represent 1  $\mu$ m in **a, c, e, h** and 100 nm in other micrographs. **(a)** Early stage WTGFP showing the large central nucleus (N) displaying two nuclear poles (NP) with cytoplasm containing a number of axonemes (A). **(b)** Detail of the cytoplasm illustrating a number of normal 9+2 axonemes (A) and abnormal axonemes. **(c)** Early stage *kinesin-13PTD* gametocytes showing the central nucleus (N) but the cytoplasm lacked visible axonemes. **(d)** Detail of the enclosed area in **c** showing randomly arranged free single and duplet MTs with some forming partial axonemes. **(e)** Late stage WTGFP showing a flagellum (F) of a developing microgamete emerging from the male gametocyte (exflagellation). N- nucleus; Ch- chromatin. **(f)** Detail of a longitudinal section through a free male gamete showing the nucleus (N) and flagellum (F). **(g)** Detail of a cross section through a male gamete showing the 9+2 flagellum and the nucleus (arrowhead). **(h)** Late-stage *kinesin-13PTD* gametocyte showing the central nucleus (N) with clumps of chromatin (Ch) but an absence of any 9+2 axonemes. **(i)** Detail of the enclosed area in **h** showing a microtubule (Mt) enclosed by the plasmalemma emerging from the male gametocyte.

**Fig 10. Summary of kinesin function throughout the *P. berghei* life cycle.** Kinesins with important roles in host and mosquito are highlighted in red.

## Supplementary Materials

### Supplementary figures

#### Fig S1. Generation and genotypic analysis of kinesin-GFP parasites

**A.** Schematic representation of the endogenous *kinesin* locus, the GFP-tagging construct and the recombined *kinesin* locus following single homologous recombination. Arrows 1 (P1) and 3 (P3) indicate the position of PCR primers used to confirm successful integration of the construct. **B.** Diagnostic PCR of *kinesin* and WT parasites using primers: integration primer (P1) and ol492 (P2). The bands of expected size for amplified DNA fragments are indicated for each tag line.

451  
452 **Fig S2. The location of kinesin-5 and kinesin-8X in relation to that of the axoneme**  
453 **marker (kinesin-8B)**

454  
455 **A.** The location of kinesin-5GFP (green) in relation to the axoneme marker, kinesin-  
456 8BCherry (red) during male gamete formation. **B.** The location of kinesin-8XGFP (green)  
457 in relation to the axoneme marker, kinesin-8BCherry (red) during male gamete formation.  
458 The nuclear location of kinesin-5 and kinesin-8X contrasts with the cytoplasmic location  
459 of kinesin-8B during chromosome replication and segregation, indicating that kinesin-5  
460 and kinesin-8X are associated with the mitotic spindle. mpa = min post activation. DNA is  
461 stained with Hoechst dye (blue). Scale bar = 5  $\mu\text{m}$ .

462  
463 **Fig S3. Generation and genotypic analysis of  $\Delta$ kinesin parasites**

464 **A.** Schematic representation of the endogenous *kinesin* locus, the targeting knockout  
465 construct and the recombined *kinesin* locus following double homologous crossover  
466 recombination. Arrows 1 and 2 indicate PCR primers used to confirm successful  
467 integration in the *kinesin* locus following recombination and arrows 3 and 4 indicate PCR  
468 primers used to show deletion of the *kinesin* gene. **B.** Integration PCR of the *kinesin*  
469 locus in WTGFP (WT) and knockout (Mut) parasites using primers: integration primer  
470 and ol248. Integration of the targeting construct gives expected size band for each gene.  
471 **C.** qRT-PCR analysis of transcript in WT-GFP and  $\Delta$ *kinesin* parasites confirming the  
472 deletion of respected genes.

473  
474 **Fig S4. Quantification of MT length in  $\Delta$ kinesin-20 and WTGFP ookinetes**

475  
476 The MT lengths were measured from the images of ookinetes stained to reveal  $\alpha$  and  $\beta$   
477 tubulins obtained by expansion microscopy. The bar diagram shows the length of  
478 subpellicular MTs in bulbous  $\Delta$ *kinesin-20* ookinetes compared to WTGFP ookinetes.  
479 Mean  $\pm$  SEM. n = 3 independent experiments.

480  
481 **Fig S5. Kinesin-13 shows co-localisation with tubulins in male gametocyte and**  
482 **gamete**

483  
484 **(A)** Indirect immunofluorescence assay showing the co-localisation of kinesin-13 (green)  
485 and tubulin staining (red) in male gamete. Scale bar = 5  $\mu\text{m}$ . **(B)** Expansion  
486 microscopy showing co-localization of kinesin-13 (green) with  $\alpha/\beta$  tubulin staining  
487 (purple) in gametocytes activated for 15 min. mpa = min post activation. Scale bar =  
488 1  $\mu\text{m}$ .

489  
490 **Fig S6. Generation and genotype analysis of conditional knockdown kinesin-  
13 parasites**

491 **(A)** Schematic representation of auxin inducible degron (AID) strategy to generate  
492 *kinesin-13AID/HA* parasites. **(B)** Integration PCR of the *kinesin-13AID/HA* construct in  
493 the *kinesin-13* locus. Oligonucleotides used for PCR genotyping are indicated and  
494 agarose gels for corresponding PCR products from genotyping reactions are shown. **(C)**  
495 Kinesin-13AID/HA protein expression level as measured by western blotting upon  
496 addition of auxin to mature purified gametocytes;  $\alpha$ -tubulin serves as a loading control.  
497 **(D)** Schematic representation of the promoter swap strategy (*kinesin-13PTD*, placing  
498 *kinesin-13* under the control of the *clag* promoter) by double homologous recombination.



499 Arrows 1 and 2 indicate the primer positions used to confirm 5' integration and arrows 3  
500 and 4 indicate the primers used for 3' integration. **(E)** Integration PCR of the promotor  
501 swap construct into the *kinesin-13* locus. Primer 1 (5'-IntPTD50) with primer 2 (5'-  
502 IntPTD) were used to determine successful integration of the selectable marker. Primer 3  
503 (3'-intClag) and primer 4 (3'-IntPTD50) were used to determine the successful integration  
504 of the *clag* promoter. Primer 1 (5'-IntPTD50) and primer 4 (3'-IntPTD50) were used to  
505 show complete knock-in of the construct and the absence of a band at 2.3 kb  
506 (endogenous) expected if no integration occurred.

507

## 508 **Supplementary Tables**

509 **Table S1.** List of genes differentially expressed between  $\Delta$ *kinesin-20* and WTGFP  
510 activated gametocytes for 2h (table S1A); and between *kinesin-13PTD* and WTGFP  
511 gametocytes (table S1B and S1C)

512

513 **Table S2.** Oligonucleotides used in this study.

## 514 **Supplementary Movies**

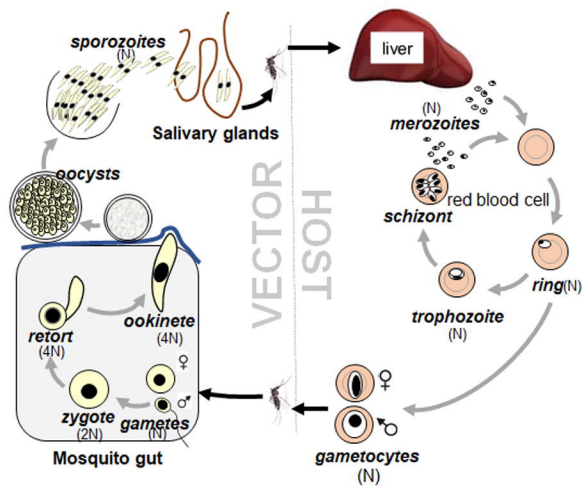
515 **Movie S1:** Gliding motility of WT-GFP ookinetes

516 **Movie S2:** Gliding motility of  $\Delta$ *kinesin-20* ookinetes

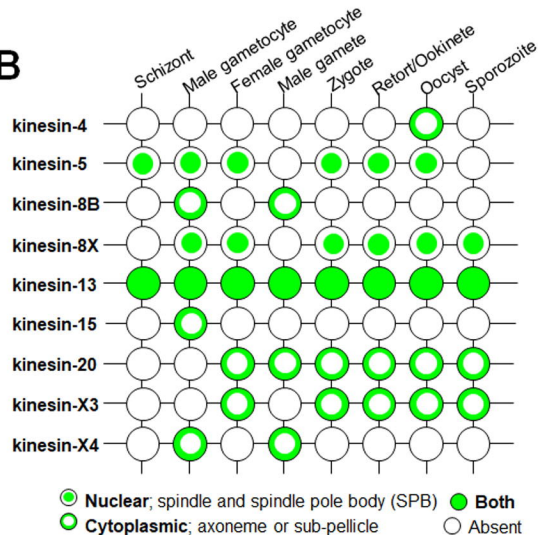
517 **Movie S3:** Gliding motility of WT-GFP salivary gland sporozoite

518 **Movie S4:** Gliding motility  $\Delta$ *kinesin-20* salivary gland sporozoite

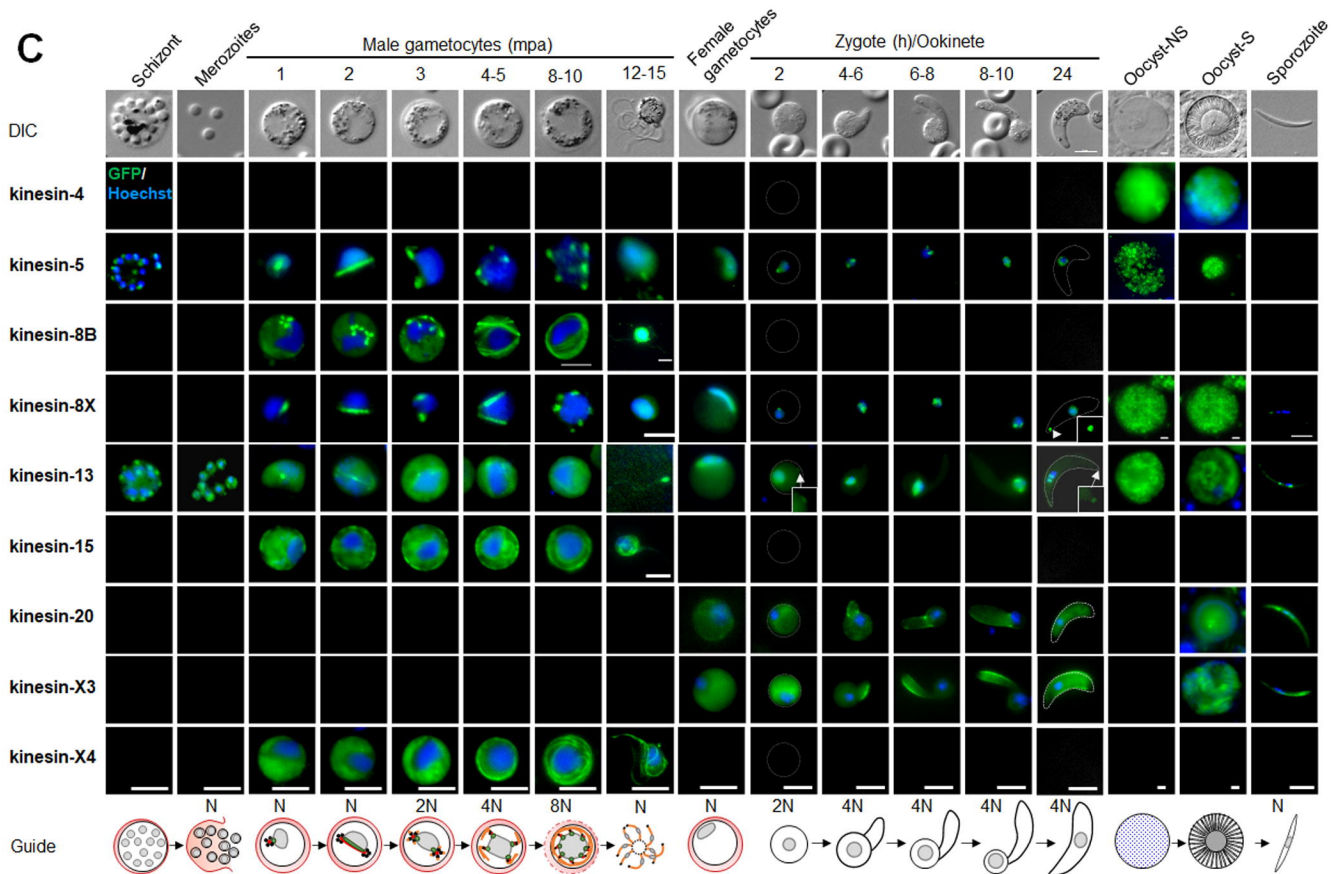
A

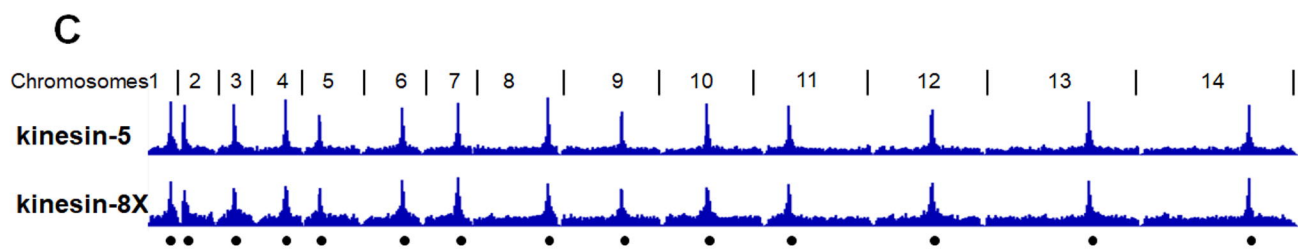
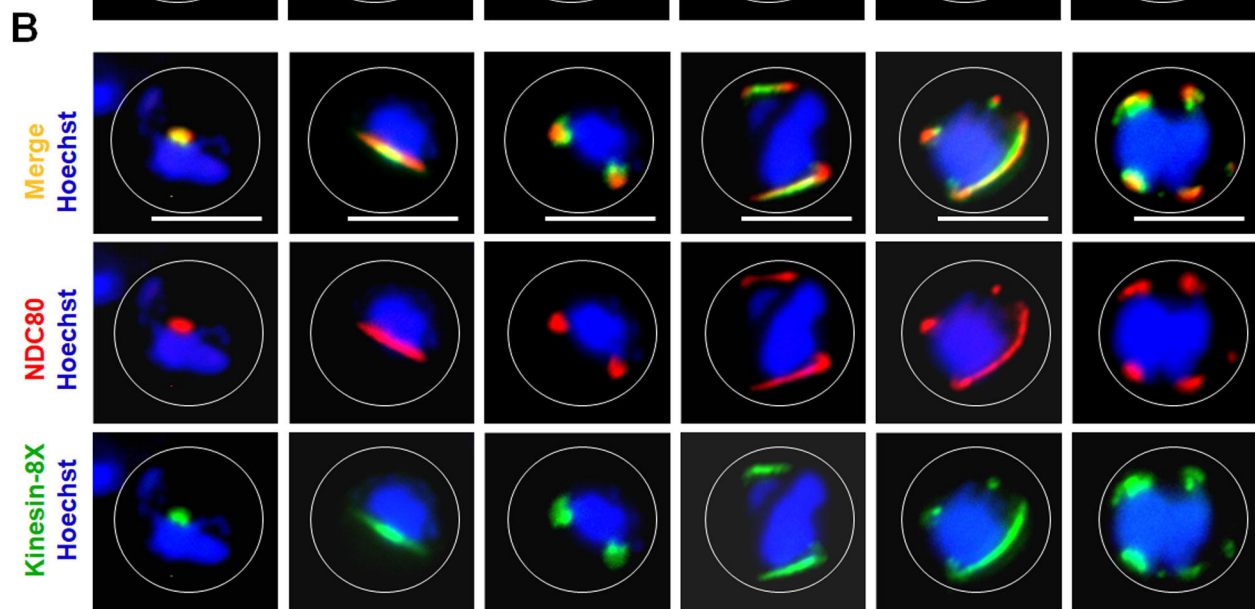
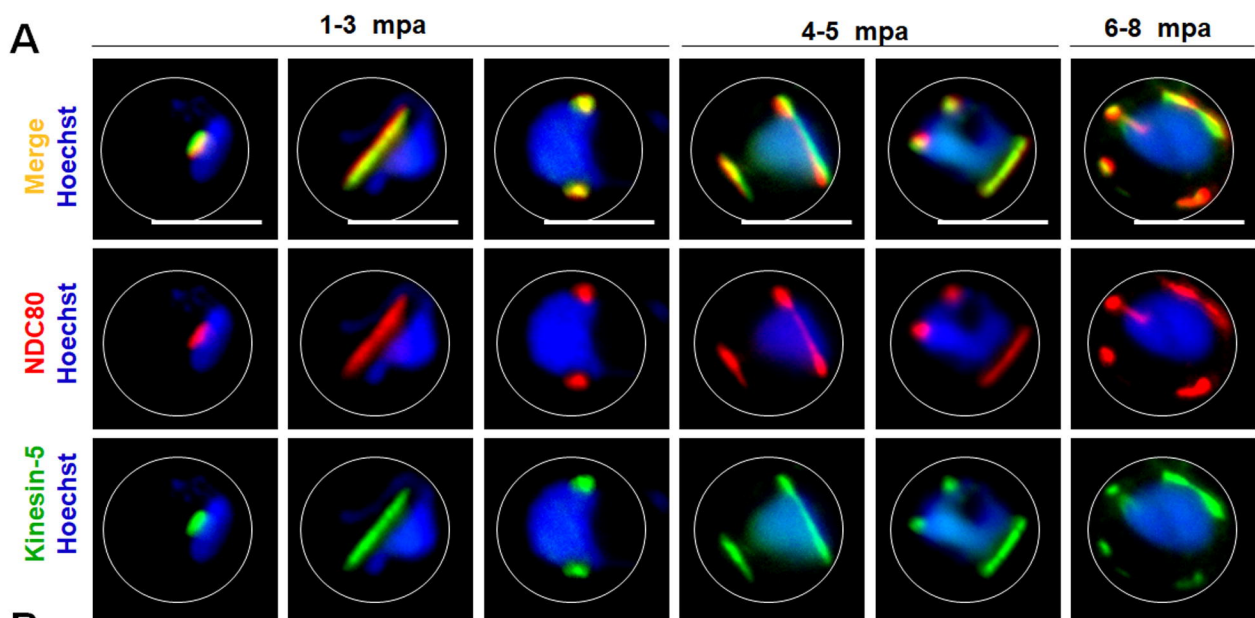


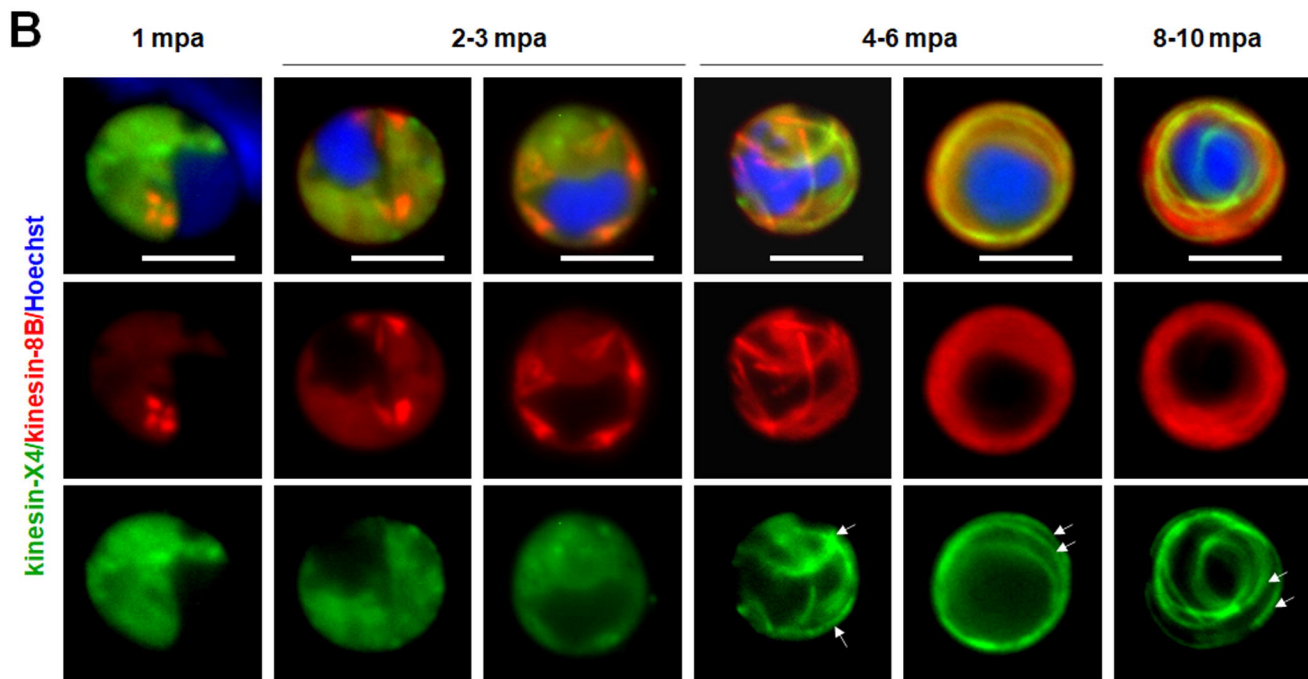
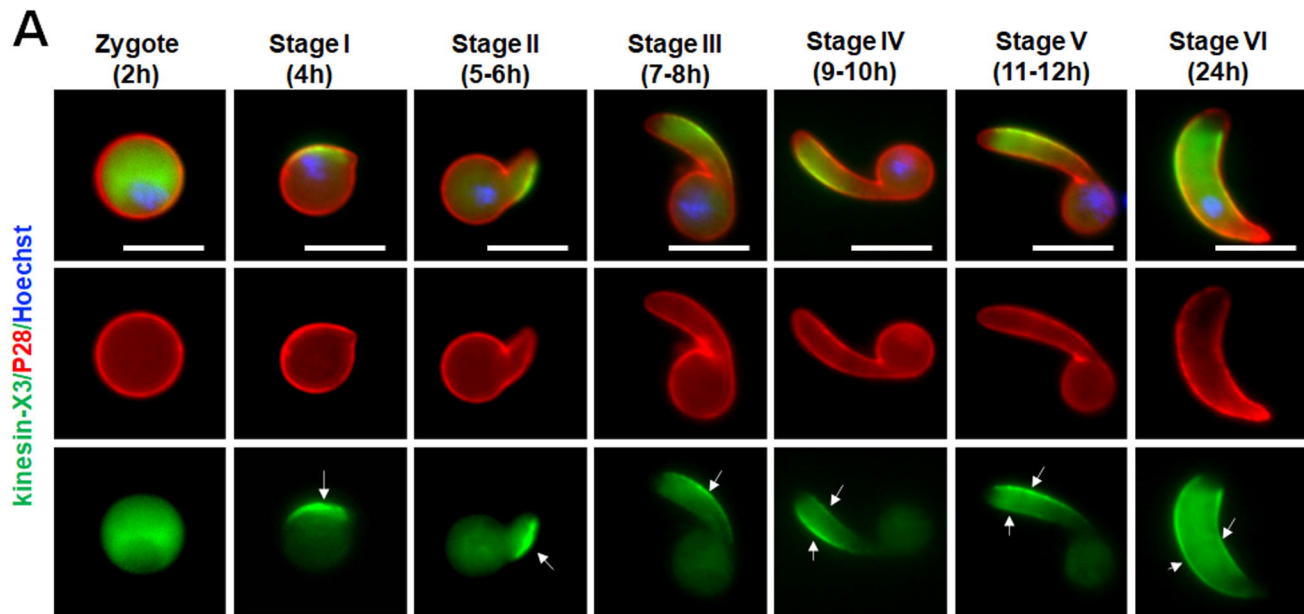
B

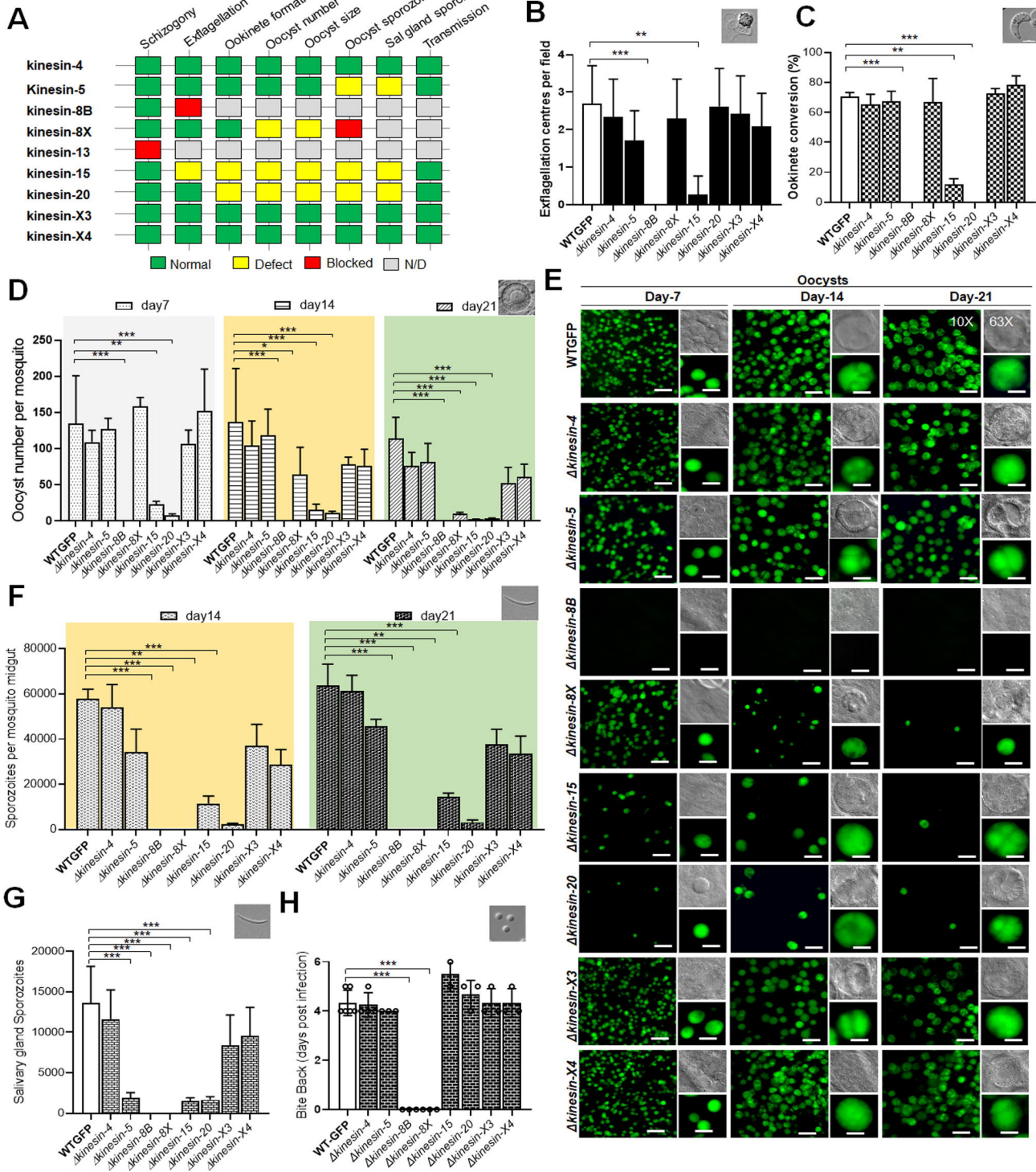


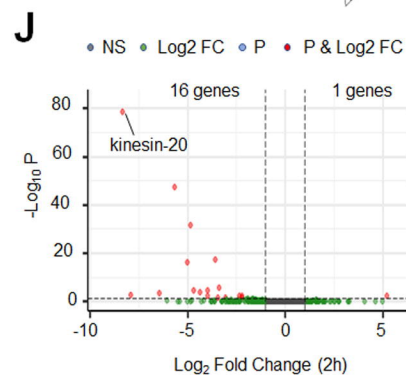
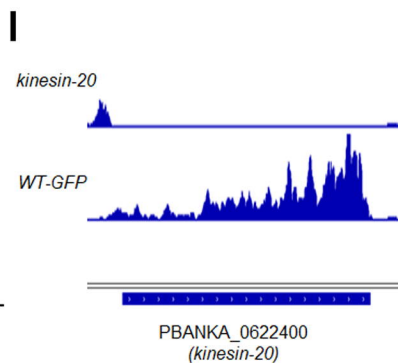
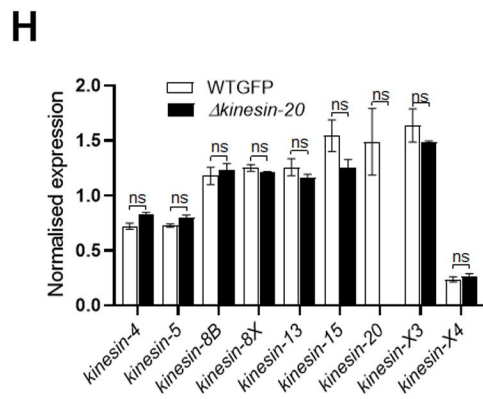
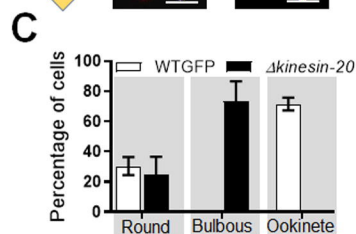
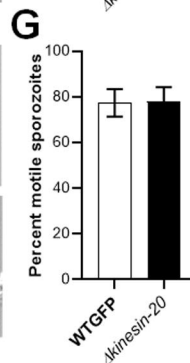
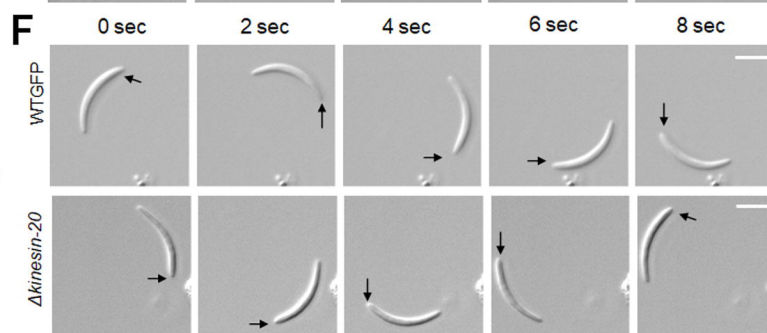
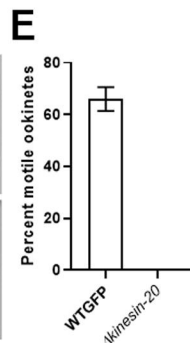
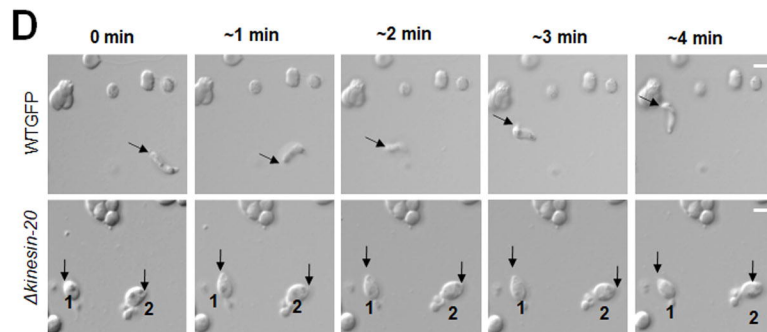
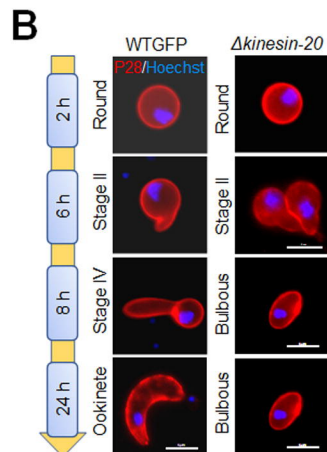
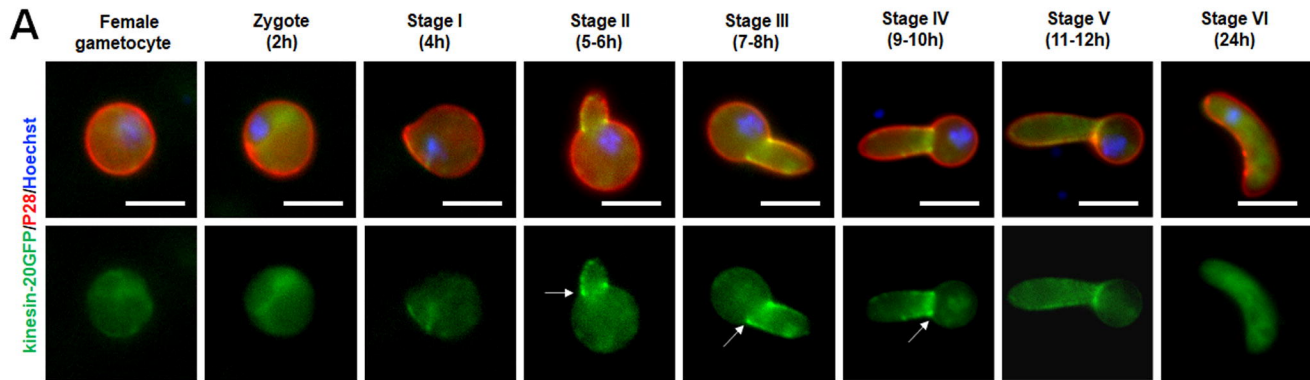
C

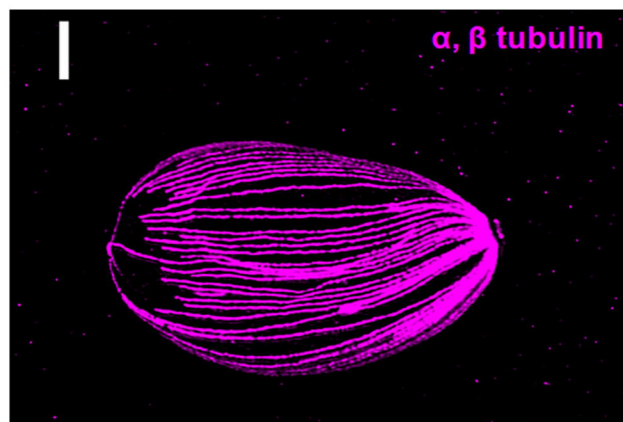
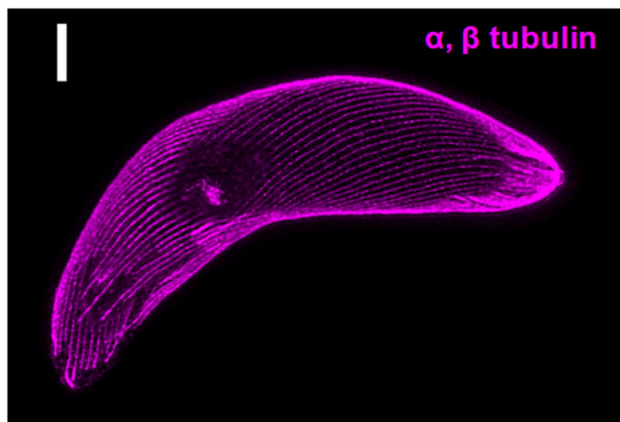
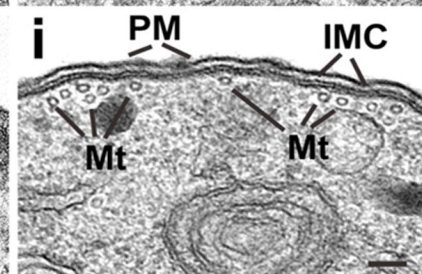
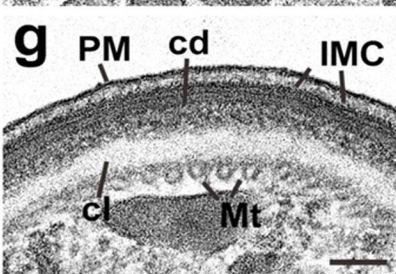
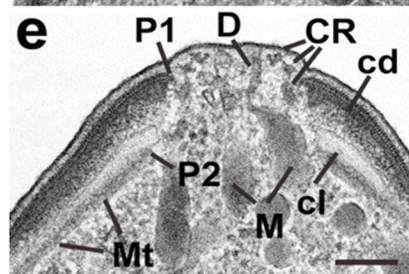
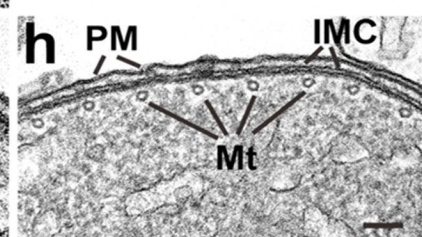
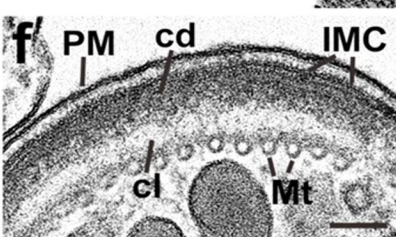
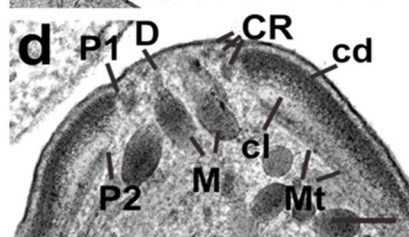
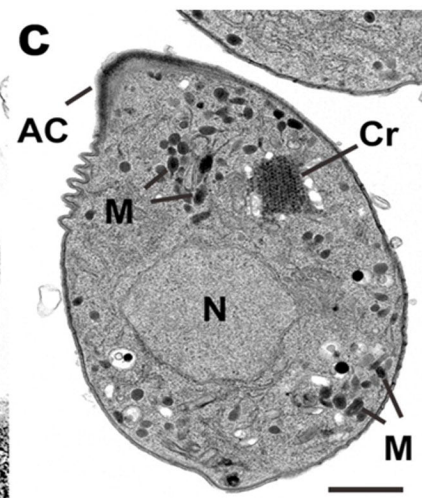
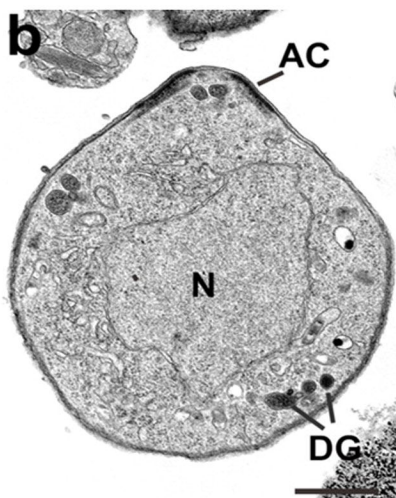
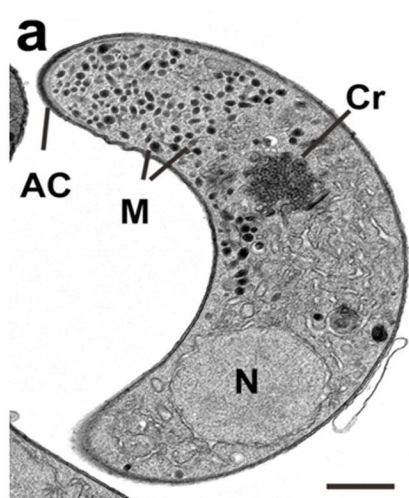




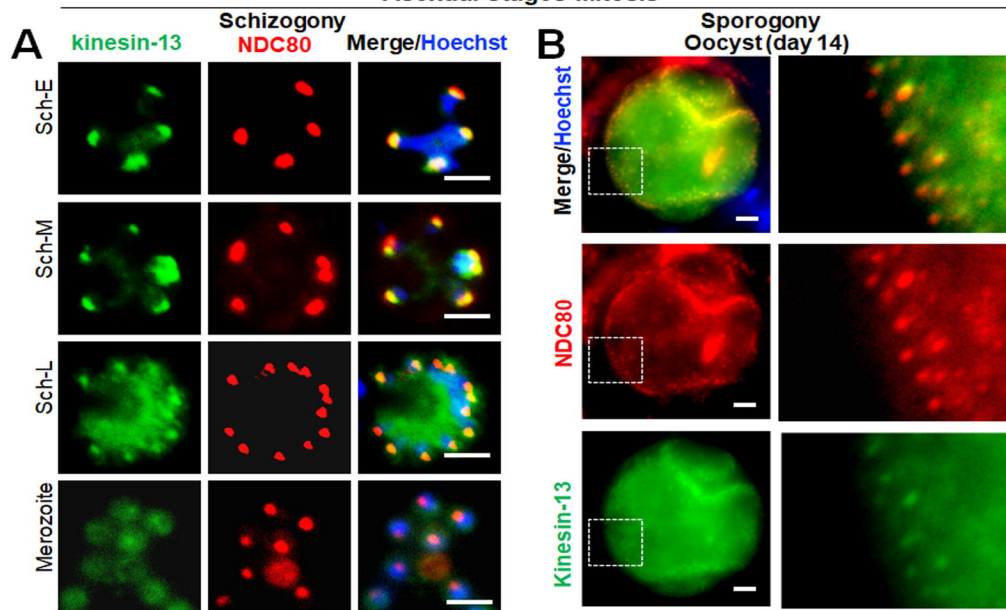




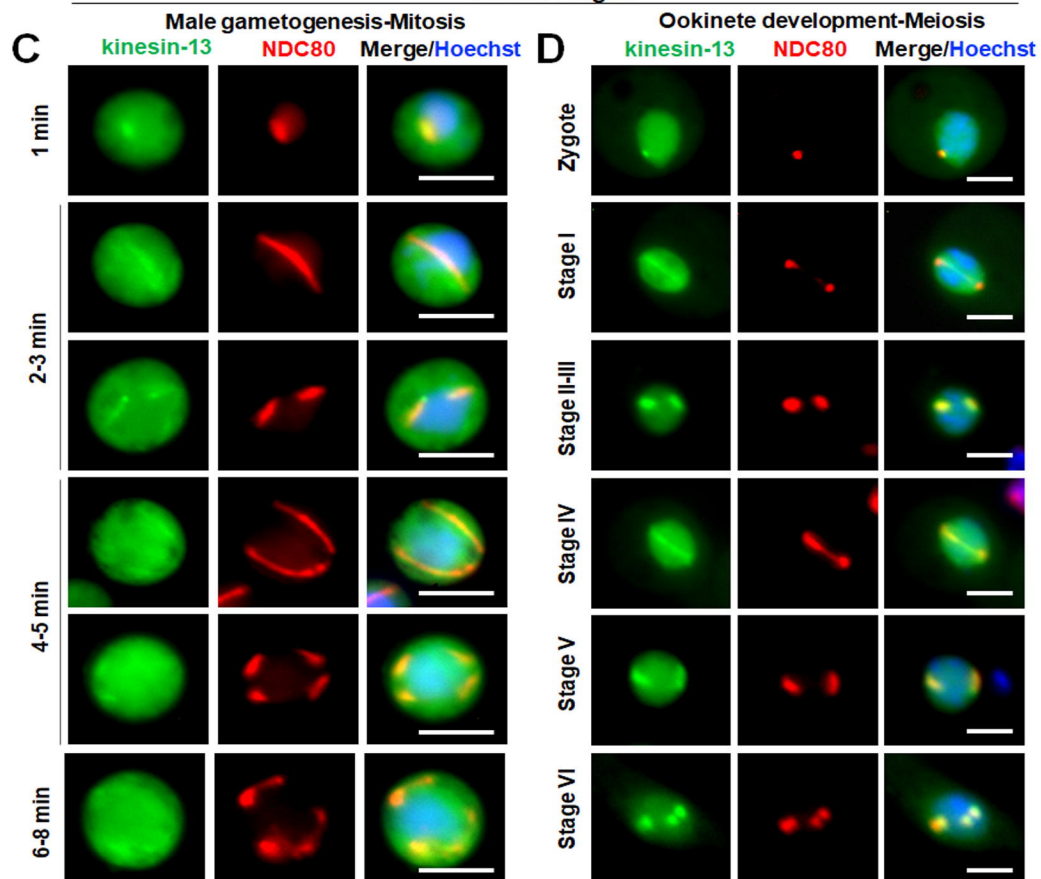


**A****WTGFP*****Δkinesin-20*****B****WTGFP*****Δkinesin-20***

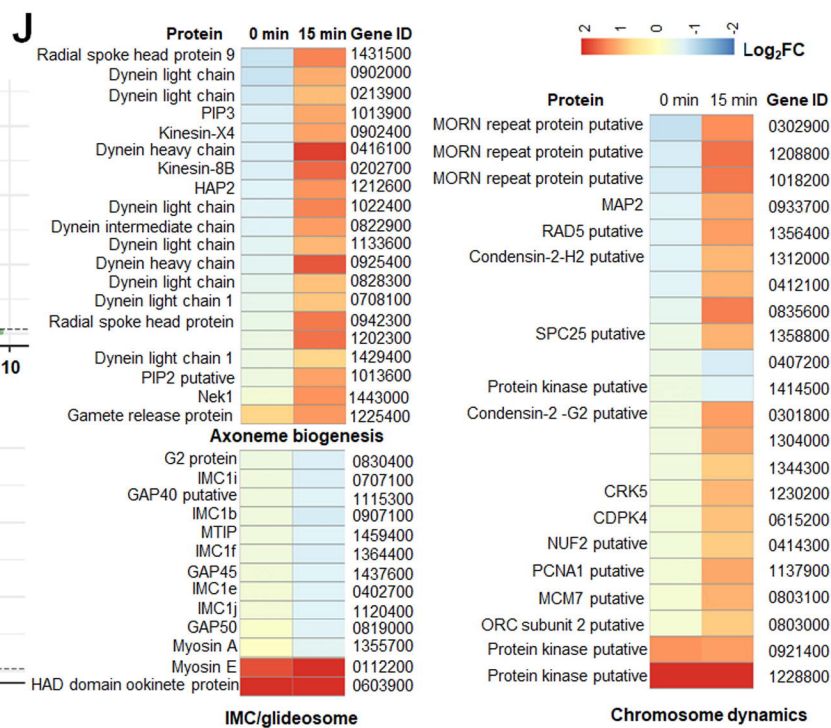
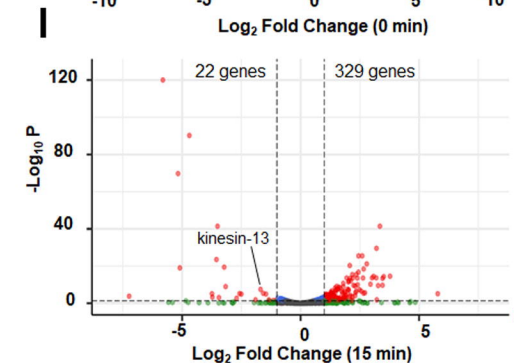
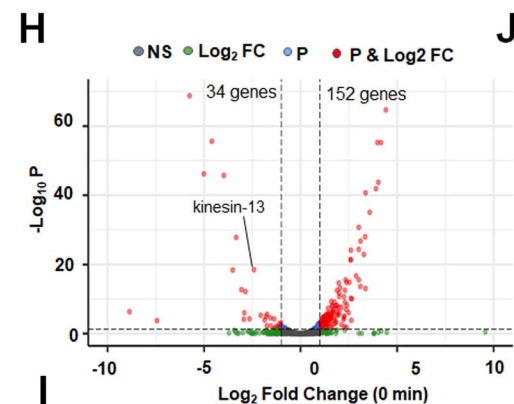
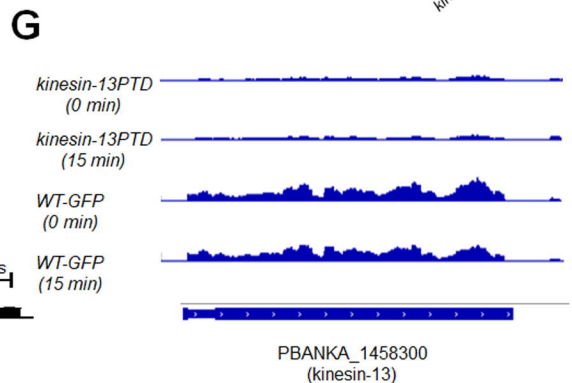
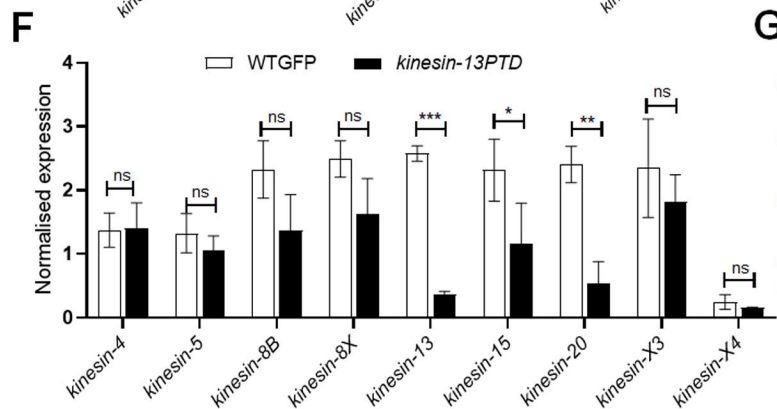
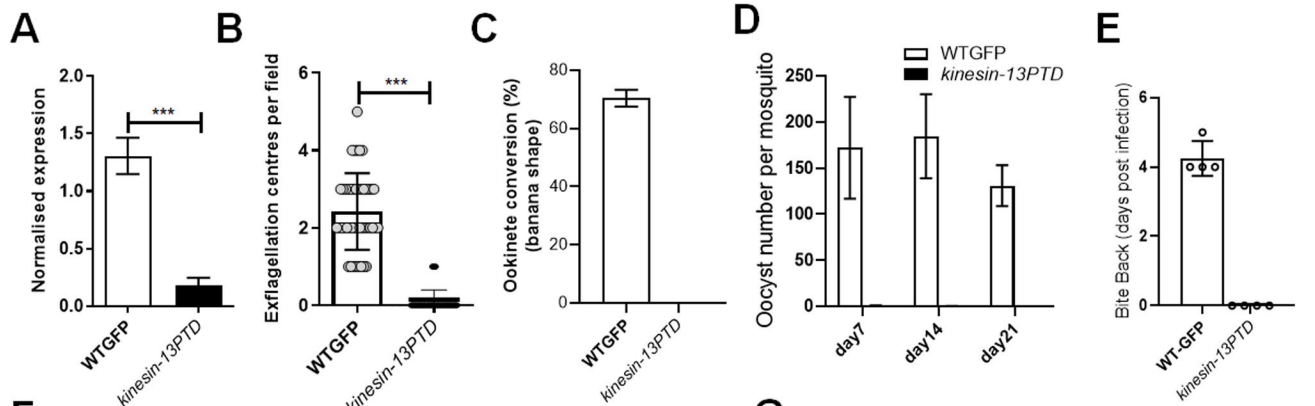
Asexual stages-Mitosis

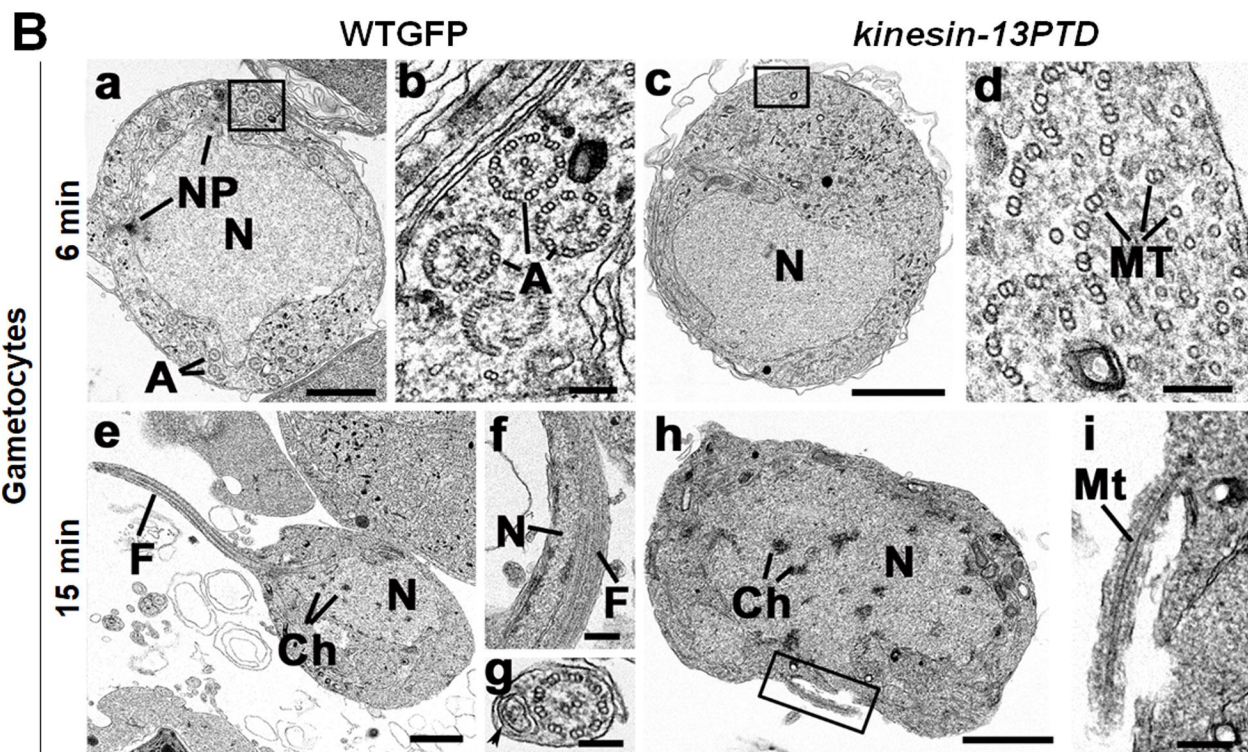
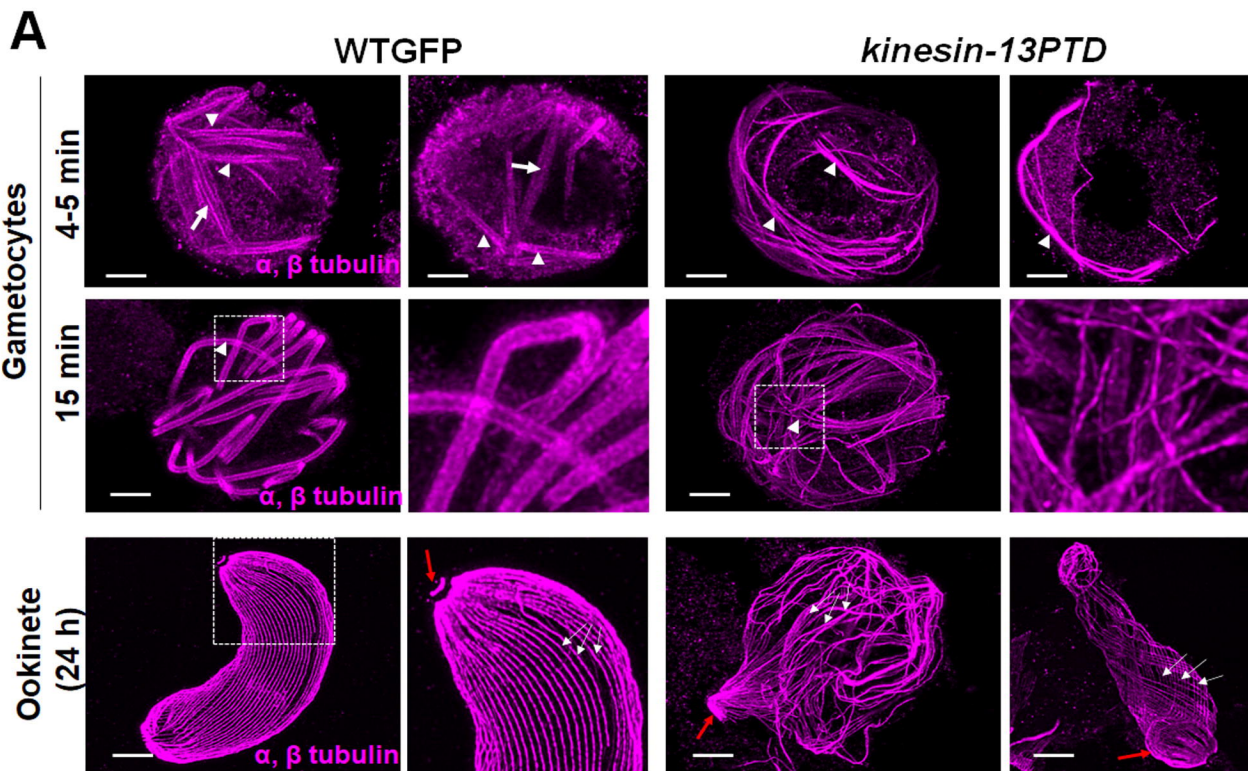


Sexual stages









# Functional Analysis of kinesins in *Plasmodium*

